Accepted Manuscript

Accumulation of progerin affects the symmetry of cell division and is associated with impaired Wnt signaling and the mislocalization of nuclear envelope proteins

Agustín Sola-Carvajal, Gwladys Revêchon, Hafdis T. Helgadottir, Daniel Whisenant, Robin Hagblom, Julia Döhla, Pekka Katajisto, David Brodin, Fredrik Fagerström-Billai, Nikenza Viceconte, Maria Eriksson

PII: S0022-202X(19)31566-0

DOI: https://doi.org/10.1016/j.jid.2019.05.005

Reference: JID 1910

To appear in: *The Journal of Investigative Dermatology*

Received Date: 10 December 2018

Revised Date: 2 May 2019

Accepted Date: 8 May 2019

Please cite this article as: Sola-Carvajal A, Revêchon G, Helgadottir HT, Whisenant D, Hagblom R, Döhla J, Katajisto P, Brodin D, Fagerström-Billai F, Viceconte N, Eriksson M, Accumulation of progerin affects the symmetry of cell division and is associated with impaired Wnt signaling and the mislocalization of nuclear envelope proteins, *The Journal of Investigative Dermatology* (2019), doi: https://doi.org/10.1016/j.jid.2019.05.005.

This is a PDF file of an unedited manuscript that has been accepted for publication. As a service to our customers we are providing this early version of the manuscript. The manuscript will undergo copyediting, typesetting, and review of the resulting proof before it is published in its final form. Please note that during the production process errors may be discovered which could affect the content, and all legal disclaimers that apply to the journal pertain.

ACCEPTED MANUSCRIPT

Accumulation of progerin affects the symmetry of cell division and is associated with impaired Wnt signaling and the mislocalization of nuclear envelope proteins

Agustín Sola-Carvajal[1,#,*], Gwladys Revêchon[1,#], Hafdis T. Helgadottir[1], Daniel Whisenant[1], Robin Hagblom[1], Julia Döhla[1, 2], Pekka Katajisto[1, 2], David Brodin[3], Fredrik Fagerström-Billai[3], Nikenza Viceconte[1], and Maria Eriksson[1,*].

[1]Department of Biosciences and Nutrition, Center for Innovative Medicine, Karolinska Institutet, Huddinge, Sweden

[2]Institute of Biotechnology, University of Helsinki, Helsinki, Finland

[3]Bioinformatics and Expression Core Facility (BEA), Karolinska Institutet, Huddinge, Sweden.

[#]Authors contributed equally

*Co-corresponding authors: Maria Eriksson and Agustín Sola-Carvajal, Department of Biosciences and Nutrition, Center for Innovative Medicine, Karolinska Institutet, NEO, Hälsovägen 7C, 14157 Huddinge, Sweden. Email: Maria.Eriksson.2@ki.se; Agustin.Sola.Carvajal@ki.se

Twitter handle: @ErikssonLab

ACCEPTED MANUSCRIPT

ABSTRACT

Hutchinson-Gilford progeria syndrome (HGPS) is the result of a defective form of the lamin A protein called progerin. While progerin is known to disrupt the properties of the nuclear lamina, the underlying mechanisms responsible for the pathophysiology of HGPS remain less clear. Previous studies in our laboratory have shown that progerin expression in murine epidermal basal cells results in impaired stratification and halted development of the skin. Stratification and differentiation of the epidermis is regulated by asymmetric stem cell division. Here, we show that expression of progerin impairs stem cells ability to maintain tissue homeostasis as a result of altered cell division. Quantification of basal skin cells showed an increase in symmetric cell division that correlated with progerin accumulation in HGPS mice. Investigation of the mechanisms underlying this phenomenon revealed a putative role of Wnt/β-catenin signaling. Further analysis suggested an alteration in the nuclear translocation of β-catenin involving the inner and outer nuclear membrane proteins, emerin and nesprin-2. Taken together our results suggest a direct involvement of progerin in the transmission of Wnt signaling and normal stem cell division. These insights into the molecular mechanisms of progerin may help develop new treatment strategies for HGPS.

ACCEPTED MANUSCRIPT

INTRODUCTION

Lamins A and C are proteins encoded by the *LMNA* gene through alternative splicing, and represent major components of the nuclear lamina, a meshwork of proteins underlying the inner nuclear membrane (Dechat et al., 2008, Prokocimer et al., 2009). Mutations in the *LMNA* gene result in disorders termed laminopathies, such as the Hutchinson-Gilford progeria syndrome (HGPS) (Dechat et al., 2008). HGPS is a rare genetic disease with multiple clinical characteristics resembling accelerated aging, including loss of subcutaneous fat, alopecia, joint stiffness, atherosclerosis and cardiovascular disease (Merideth et al., 2008, Strandgren et al., 2017). Most HGPS patients present a *de novo* point mutation in the *LMNA* gene (c.1824C>T, p.G608G), which activates a cryptic splice site resulting in a truncated and impaired post-translationally modified protein called progerin (De Sandre-Giovannoli et al., 2003, Eriksson et al., 2003). Progerin accumulates at the inner nuclear lamina and disrupts its properties, causing the characteristic nuclear blebbing and a variety of cellular defects, including epigenetic modifications, senescence, and DNA repair deficiency (Kubben and Misteli, 2017). However, the molecular mechanisms by which progerin leads to premature aging remain unclear.

A proposed model to explain the HGPS disease mechanisms suggests that adult stem cells undergo premature exhaustion and therefore, the capacity of these cells to regenerate and maintain tissue homeostasis is reduced (Halaschek-Wiener and Brooks-Wilson, 2007, Rosengardten et al., 2011, Scaffidi and Misteli, 2008). The effects of this reduced capacity of stem cells is most significant in tissues that have a high degree of cell turnover, like in the skin. In addition, previous results from our lab have shown that postnatal expression of the HGPS mutation in epidermal basal cells

results in a decreased population of adult stem cells and impaired wound healing (Rosengardten et al., 2011). We also showed that embryonic expression of the HGPS mutation results in halted skin development (McKenna et al., 2014). In mice, the epidermis develops as a multilayered epithelium that is generated by perpendicular divisions of stem cells in the basal layer and skin homeostasis is sustained by a series of asymmetric and symmetric cell divisions. (Lechler and Fuchs, 2005). Asymmetric stem cell division (ACD) generates a new stem cell, which remains in the basal layer, and a daughter cell committed to differentiation, which migrates upwards to the suprabasal layer. On the contrary, symmetric stem cell division (SCD) leads to the production of two daughter stem cells. Interestingly, mutations in genes encoding lamins and proteins of the nuclear envelope (NE) have been shown to result in defects in nuclear positioning, cell polarization, and migration (Lombardi and Lammerding, 2011). Moreover, interactions between the nuclear lamina and NE proteins, such as emerin, and nesprin-2, play an essential role in the transmission of signals and stimuli via the cytoskeleton to the nucleus.

In this study, we demonstrated that expression of progerin interferes with the normal development of the interfollicular epidermis (IFE) and the ability to maintain skin homeostasis, through abnormal stem cell division. We used our previously described conditional HGPS mouse model with continuous expression of progerin in the skin from embryogenesis and onwards (McKenna et al., 2014) to analyze the potential effects of altered stem cell division. To further characterize this model, we performed global transcriptomic analysis of isolated keratinocyte subpopulations. Our results suggest a model in which the expression of progerin in the nuclear lamina progressively alters the normal crosstalk of signals between nucleus and cytoplasm by

interfering with NE proteins. As a consequence, key signaling pathways such as the Wnt/β-catenin signaling pathway are misregulated, resulting in the alteration of essential cellular processes, such as stem cell division and maintenance of stemness.

RESULTS

Epidermal stem cells shift towards symmetric cell division as progerin accumulates

Skin development occurs through stratification of the epidermis, and is partly mediated by asymmetric cell division. In skin, ACD can be assessed by the polarity of basal epidermal cells during division (Lechler and Fuchs, 2005). Epidermal cell division is considered asymmetric when basal cells divide perpendicularly to the basement membrane, whereas symmetric cell division occurs when cells divide parallel to the basement membrane. Hence, we first analysed the orientation of the mitotic spindle to determine the direction of division *in vivo* (Figure 1a). Using antibodies against tubulin and keratin 5 on dorsal skin sections, we could visualize the orientation of the mitotic spindles and determine their angle relative to the basement membrane in dividing basal keratinocytes (Figure 1a-c). At both embryonic day 18.5 (E18.5) and post-natal day 4 (PD4), wild-type mice displayed similar distributions of the two mitotic spindle orientations. Contrastingly, at E18.5, HGPS skin showed a higher frequency of epidermal cells dividing parallel to the basement membrane compared to wild-type (42.9% *vs*. 30% respectively) (Figure 1b, d). This phenomenon was further emphasized at PD4, where 66.7% of the cells were found to divide parallel to the basement membrane (compared to 42.2% in age-matched wild-type) (Figure 1c, d). This imbalance in the polarity of cell division correlates with the progressive accumulation of progerin that we previously reported in this model

(McKenna et al., 2014). Hence, the observed shift towards SCD suggests an abnormal proliferative capacity of basal keratinocytes, which may in part be responsible for the halted skin development seen in our HGPS mice.

Altered stem cells in HGPS mouse skin

The balance between ACD and SCD is an important process regulating skin homeostasis and morphogenesis, as it accounts for the maintenance of a constant stem cell pool. We next investigated whether progerin expression had an impact on stem and progenitor cells. To this end, keratinocytes from PD4 HGPS and wild-type mice were extracted and the basal and suprabasal populations sorted by FACS using markers against α6-integrin and CD45 (Figure S1a). RNA from these populations was isolated and processed for RNA sequencing to identify differentially expressed genes in HGPS and wild-type mice. Cufflinks analysis revealed that 308 genes in basal keratinocytes and 82 genes in suprabasal keratinocytes differed significantly (false discovery rate (FDR) < 0.1). Among the top 20 most abundant gene ontology (GO) terms, processes including epidermis and skin development, as well as the regulation of cell differentiation, were significantly affected in HGPS (Figure S1b and Table S1). Several of these processes were also affected in suprabasal keratinocytes, but to a lesser extent (Table S1). Different lineages of proliferative keratinocytes have been identified in mice IFE. These are known as label-retaining cells (LRCs) and non-label-retaining cells (nLRCs) and represent two stem cell populations characterized by specific proliferative and differentiation capacities (Sada et al., 2016). Similarly, in mice hair follicles (HF), proliferative keratinocytes have been identified as two distinct types of stem cells (HFSCs) and as progenitor/transit-amplifying cells (TACs) (Hsu et al., 2014). We applied previously established gene expression patterns for

these different cell lineages to our RNA sequencing data (Jaks et al., 2008, Morris et al., 2004, Nowak et al., 2008, Rezza et al., 2016, Sada et al., 2016, Troy et al., 2011), and found several genes that were markedly affected by progerin expression. Gene expression patterns associated to LRCs, HFSCs and TACs were particularly downregulated in HGPS keratinocytes (Figure S1c, d and Table S2). Expression array data were used to validate the gene expression changes observed with RNA sequencing in HGPS keratinocytes (Figure S1e, f and Table S2). We then performed *in situ* hybridization against keratin 15 (K15), a marker of HFSCs found significantly downregulated in HGPS basal keratinocytes, to investigate whether the alteration of gene expression could also be observed during embryonic development (Figure S1g). Quantification revealed that K15 was found in both HF and IFE in wild-type mice, but was almost undetectable in HGPS mice. The notable decrease in K15 was visible already at E18.5 and at PD4 in HGPS compared to wild-type skin (Figure S1h). Taken together, these observations suggest an effect on epidermal stem cell function due to the detected changes in the transcriptome.

Progerin expression is associated with increased keratinocytes proliferation

To determine whether the downregulation of LRC and HFSC genes had an impact on stem cell characteristics such as the proliferative or quiescent state, we first considered the signatures of genes known to be involved in such processes (Figure 2a and Table S3). A total of 61.5% of genes associated with proliferation were found significantly misregulated in HGPS basal keratinocytes. On the contrary, significant changes in gene expression levels associated with quiescence accounted for 25% of the dataset in HGPS (Figure 2a and Table S3). Taken together, these results suggest a more proliferative state for epidermal cells in HGPS compared to wild-type. We

subsequently assessed cell proliferation by immunohistochemistry against the mitotic marker PHH3 (Figure 2b). Analysis showed a significantly higher frequency of dividing cells in the basal layer of HGPS IFE. Surprisingly, cells were also found to proliferate in the suprabasal layer of HGPS IFE, while this phenomenon was largely absent in wild-type skin (Figure 2b, c). Similarly, PHH3 was also more present in HGPS HF (Figure 2d). As the equilibrium between proliferation and differentiation plays a fundamental role in skin homeostasis, we then investigated expression changes in established epigenetic regulators of epidermal differentiation. Indeed, epigenetic modifiers participate in the coordination of cell proliferation and differentiation, by regulating stemness and cell-commitment genes (Perdigoto et al., 2012). Analysis of differentially expressed genes between wild-type and HGPS skin revealed no major changes in the expression of epigenetic modifiers in either basal and suprabasal keratinocytes (Figure S2a, b). This indicates that progerin expression does not interfere with the proliferation/differentiation switch at the epigenetic level in these HGPS mice. These data further emphasize our previous observations, that HGPS skin presents a disrupted homeostasis, likely as a result of an alteration of stem cells' functions.

Impaired Wnt/β-catenin signaling pathway upon progerin expression

Several signaling pathways are involved in the maintenance of stem cells equilibrium in developing hair follicles and IFE, including Hedgehog (HH), Notch and Wingless (Wnt). We next addressed the question of which pathways could be associated with the loss of balance in ACD *vs.* SCD. Pathway analysis using Wikipathway pointed to Wnt signaling as the most significantly affected pathway in HGPS skin ($p < 0.05$). Notch, as well as the transforming growth factor signaling pathways TGF-β, also

seemed to be impacted by progerin expression but to a lesser extent (Table S4). We then specifically considered misregulations in Wnt, Notch and HH pathways in HGPS skin using our RNA sequencing data. For all three pathways, genes were found to be mainly downregulated in basal keratinocytes, with the Wnt pathway being the most significantly affected by progerin expression (Figure S3a and Table S5). This was also observed in suprabasal keratinocytes (Figure S3b and Table S5). The majority of the downregulated genes identified with RNA sequencing in HGPS keratinocytes were validated by expression array analysis (Figure S3c, d and Table S5). The canonical Wnt/β-catenin signaling pathway has previously been found to regulate stem cell renewal in an autocrine manner in mouse IFE (Lim et al., 2013) and has also been implicated in HGPS (Choi H. et al., 2018, Choi J. Y. et al., 2018, Hernandez et al., 2010). To validate our findings, we primarily made use of dermal fibroblasts from HGPS patients. The alteration of the Wnt/β-catenin pathway was confirmed in patient fibroblasts using immunofluorescence (Figure 3a). Indeed, nuclear β-catenin levels were reduced in HGPS fibroblasts compared to controls, which was visible at both early and late passages (Figure 3b). Patient and control fibroblasts were stimulated with Wnt3a over a 24-hour time course to determine whether the Wnt/β-catenin pathway defect was reversible. Western blot analysis showed an increase in nuclear β-catenin levels over time, peaking after stimulation for 16 hours for control and 24 hours for HGPS fibroblasts (Figure S4a, b). Quantification of nuclear active β-catenin fluorescence intensity after 8 hours of stimulation also suggested a partial increase in the protein levels in both control and HGPS fibroblasts (Figure S3c, d). Similarly, expression levels of Axin2, a Wnt target gene, showed up to a 5-fold increase after stimulation (Figure S3e). However, both active β-catenin and Axin2 levels remained lower in HGPS than in control fibroblasts, further emphasizing the impairment of the

canonical Wnt/β-catenin signaling pathway in HGPS. We then investigated whether this could be observed specifically in the IFE of our HGPS mouse model. Importantly, assessment of β-catenin fluorescence intensity revealed a significant reduction in nuclear β-catenin in PD4 HGPS IFE compared to wild-type (Figure 3c, d). Together, these results suggest an important role of the canonical Wnt/β-catenin signaling pathway in the phenotype observed in our HGPS mouse model.

Dysregulation of emerin and nesprin-2 in HGPS skin

The results described above argue for an impaired nuclear transportation of β-catenin in our model. Indeed, two NE proteins, emerin and nesprin-2, were previously found to be involved in such process. Emerin was suggested to participate in β-catenin export from the nucleus while nesprin-2 was found necessary to the nuclear translocation of β-catenin (Markiewicz et al., 2006, Neumann et al., 2010). Thus, we next investigated the effects of progerin on emerin and nesprin-2 protein dynamics. We first assessed nuclear levels of emerin by immunofluorescence in HGPS and wild-type mice IFE at E18.5 and PD4. Fluorescence intensity analysis showed no differences in emerin levels between wild-type and HGPS mice at E18.5, however, emerin was found significantly increased in HGPS IFE at PD4 (Figure 4a, b). Intensity profiles demonstrated that this increase was most apparent at the nuclear rim (Figure 4c). To rule out the possibility that the increase in emerin levels was a consequence of overexpressing both lamin A and progerin, we used the same analysis in a mouse model overexpressing only lamin A. Emerin staining was similar to wild-type levels in mice overexpressing lamin A, which suggested that emerin may interact more specifically with progerin than lamin A (Figure 4a-c). In parallel, we determined whether progerin expression was interfering with nesprin-2. Staining analysis of

HGPS and control fibroblasts revealed a decrease in nuclear nesprin-2 in HGPS patient cells at both early and late passages (Fig 5a, b). Furthermore, the reduction was not solely observed in the whole nucleus, but also at the nuclear rim (Figure 5b). Our data provide evidence that expression of progerin impedes the normal dynamics of emerin and nesprin-2. The impaired localization of these two proteins suggests a higher exportation rate of β-catenin from the nucleus, which in turn may result in the downregulation of the Wnt/β-catenin signaling pathway and disrupted stem cell function.

DISCUSSION

HGPS is a genetic disorder arising from the accumulation of progerin, a toxic protein integrated in the nuclear lamina. How progerin expression induces defects in molecular and cellular processes resulting in premature aging-like symptoms remains largely unclear. Over the years, several hallmarks of progeroid syndromes have been established, including stem cell exhaustion, and several studies have suggested that deficiencies in HGPS stem cells could impair tissue development and homeostasis (Carrero et al., 2016, Halaschek-Wiener and Brooks-Wilson, 2007, Rosengardten et al., 2011, Scaffidi and Misteli, 2008).

In this study, we used a humanized mouse model expressing the most common HGPS mutation specifically in basal keratinocytes, to provide evidence for a mechanism in which HGPS stem cells fail to maintain tissue homeostasis through impaired stem cell regeneration. As a result, we showed that basal keratinocytes from HGPS mice favored SCD over ACD *in vivo*. This imbalance was already evident during late stages of embryonic development and became significantly more pronounced

postnatally, as progerin accumulated. It was previously found that overexpression of progerin in neural stem cells leads to intrinsic SCD *in vitro*, though the brain of HGPS patients is protected from progerin's deleterious effects (Moore et al., 2015). In line with our data, this suggests that progerin is able to impact the fate determinants of dividing stem cells, both through extrinsic and intrinsic mechanisms. In 2005, Lechler and Fuchs found that most cell divisions occurring in wild-type mice epidermis were asymmetric from E15.5 onwards. They also showed that p63-null mice, which display a deficient skin development, had an overrepresentation of cells with symmetric divisions (Lechler and Fuchs, 2005). It is interesting to note that progerin-expressing keratinocytes were previously found to exhibit a reduction in p63 (Rosengardten et al., 2011). Taken together, this further supports our results that expression and accumulation of progerin lead to a shift towards SCD.

There have been debates as to the identity of stem/progenitor cells composing the epidermis, with no predominant model to explain epidermal maintenance (Mascre et al., 2012, Rezza et al., 2016, Rompolas et al., 2016, Sada et al., 2016). Here, we applied the gene expression pattern from the two stem cell populations-model (LRCs and nLRCs) proposed by Sada et al. characterizing IFE proliferative keratinocytes, as well as the markers established by Rezza et al. to identify HFSCs and TACs in HF. Our RNA sequencing data showed a downregulation of stem and progenitor cell markers in HGPS epidermis. We further found by *in situ* hybridization that K15 downregulation in both IFE and HF of HGPS mice correlates with the excessive SCD indicating that stem/progenitor cell functions might be affected already during embryonic development.

The bases for tissue development and homeostasis reside in the proliferation of stem and progenitor cells, and our data pointed to an aberrant proliferation mechanism. Indeed, some of the genes that were found to be downregulated, such as Igfbp3, Wnt6 and Nfatc1, have previously been linked to keratinocytes proliferation *in vivo* (Edmondson et al., 2005, Horsley et al., 2008, Mendoza-Reinoso and Beverdam, 2018). On the other hand, in other reports, K15 expression was suppressed in non-homeostatic, hyperproliferating conditions, such as in psoriatic tissues or during wound healing (Jia et al., 2016, Porter et al., 2000, Waseem et al., 1999). In accordance, we found that basal cells of the IFE and HF divided at a higher rate, while IFE suprabasal cells were also found to divide in HGPS epidermis. Progerin-expressing cells are characterized by a loss of heterochromatin, in particular the histone H3 trimethylated on lysine 27 (H3K27me3) (Goldman et al., 2004, Shumaker et al., 2006). Trimethylation of H3K27 occurs via the epigenetic modifier EZH2, a known regulator involved in keratinocytes proliferation and differentiation (Ezhkova et al., 2009, Shumaker et al., 2006). However, in contrast with the *in vitro* data presented by Shumaker and colleagues, we did not find epigenetic regulators, such as EZH2, to be affected in our HGPS mice (Shumaker et al., 2006). Our data suggest that even though there is an expansion of the basal keratinocytes in HGPS, progerin-expressing keratinocytes are able to switch from a proliferative state to a differentiating state. In accordance, a previous study conducted on these HGPS mice showed expression of epidermal terminal differentiation markers in suprabasal layers of the IFE (McKenna et al., 2014). Therefore, as progerin-expressing basal keratinocytes favor SCD, the pool of actively dividing cells may be largely expanded, thereby reducing the fraction of differentiating cells and resulting in a non-homeostatic tissue

Wnt and Notch signaling pathways were previously found impaired in both *in vitro* and tissues derived from *in vivo* models of HGPS, with this impairment thought to contribute to the alteration of stem cells functions (Choi H. et al., 2018, Choi J. Y. et al., 2018, Espada et al., 2008, Hernandez et al., 2010, Rosengardten et al., 2011, Scaffidi and Misteli, 2008, Schmidt et al., 2012). In this study, we provide further evidence for such a phenomenon, adding emphasis on the canonical Wnt/β-catenin pathway in the IFE since Wnt signaling has previously been associated with ACD (Habib et al., 2013, Ouspenskaia et al., 2016). Indeed, Ouspenkaia and colleagues showed that cells with low Wnt signaling divided symmetrically during HF formation, reinforcing our hypothesis that loss of Wnt signaling results in aberrant orientation of cell division.

The NE proteins emerin and nesprin-2 were shown to intrinsically influence β-catenin activity, either by regulating its access to the nucleus or by facilitating its nuclear translocation (Markiewicz et al., 2006, Neumann et al., 2010). Progerin was described as interacting directly with emerin, while nesprin-2 is an indirect interactor of both lamin A/C and emerin (Chojnowski et al., 2015, Kubben et al., 2010, Libotte et al., 2005, Vaughan et al., 2001, Zhang et al., 2005). Overexpression of the nesprin-2 KASH domain has been shown to be beneficial in progerin-expressing aortic smooth muscle cells and in HGPS mice (Kim et al., 2018). These studies further emphasize the connection between progerin and NE proteins. In our study, these protein dynamics were found to be affected by progerin expression, with nuclear accumulation of emerin and reduction of nesprin-2, in agreement with previously reported *in vitro* data (Arsenovic et al., 2016). This suggests that the loss of nuclear β-

catenin in HGPS keratinocytes may be the result of active exportation by emerin and inactive translocation by nesprin-2. However, nesprin-2 reduction remains unclear and further studies are needed to explain how progerin expression leads to its mislocalization. Progerin was previously found to interact with SUN1, an inner nuclear membrane protein and interactor of nesprin-2, resulting in SUN1 aggregation at the NE (Chen et al., 2012, Chen et al., 2014, Padmakumar et al., 2005). Disruption of the SUN-nesprin interaction was found to lead to nesprins diffusion (Padmakumar et al., 2005). Hence, accumulation of SUN1 in HGPS cells may reduce its interaction with nesprin-2, resulting in nesprin-2 mislocalization. That several studies suggest that emerin and nesprins influence polarity during cell division is also noteworthy. While emerin interacts with microtubules necessary for centrosomes localization to the nuclear envelope, lamins A/C are required for proper localization of emerin at the inner nuclear membrane, suggesting roles for these proteins in cell polarity (Libotte et al., 2005, Salpingidou et al., 2007, Zhang Q. et al., 2005).

In conclusion, we propose a model in which progerin, through its potential direct interaction with emerin, may alter nesprin-2 localization indirectly, which distorts the Wnt/β-catenin signaling pathway. This may lead to an aberrant stem cell division characterized by impaired polarity and increased proliferation, impeding epidermal development and homeostasis, which in turn results in stem cell exhaustion (Rosengardten et al., 2011). Here we provide evidence that defects in the nuclear lamina could affect cellular processes such as the symmetry of cell division, and further highlight the probable role of NE proteins in such mechanisms in the skin. These findings may provide perspectives for the development of new treatment strategies for progeria and age-associated diseases.

MATERIALS & METHODS

Transgenic mice

Animal studies were approved by the Stockholm South Ethical review board (Dnr. 35-15). All procedures were performed in accordance with the institutional guidelines and regulations. Heterozygous tetop-LA^{G608G} or tetop-LA^{wt} (Sagelius et al., 2008) mice were intercrossed with heterozygous K5-tTA mice (Diamond et al., 2000). Throughout the paper, tetop-LA^{G608G+}; K5-tTA^{+} mice are referred to as HGPS. Non-transgenic littermates are referred to as wild-type.

Immunostainings

HGPS and unaffected primary dermal fibroblasts were obtained from the Coriell Cell Repositories (Camden, NJ, USA). Tissue and cell immunostainings were done as previously described (Revêchon et al., 2017). The following primary antibodies were used: anti-keratin 5 (PRB-160P; BioSite), anti-alpha tubulin (Abcam), anti-beta catenin (CAT-15, ThermoFisher Scientific), anti-progerin (mAb 134A, Enzo Life Science), anti-emerin (NCL-Emerin, Leica), anti-phospho-Histone H3 (Ser 10, Millipore), anti-beta catenin (CAT-15, Invitrogen), anti-active beta catenin (8E7, Merck Millipore), and anti-nesprin-2 MANNES2G (4B5, Randles et al., 2010).

Statistical analysis

Unpaired Student's t-tests with a two-tailed 95% confidence interval was used. ACD groups comparison was performed using Fisher's exact test, Bonferroni adjustments. Significance was defined as *$p < 0.05$; **$p < 0.005$.

Data availability

The datasets are available in the Gene Expression Omnibus repository (accession number GSE131311). The authors declare that all data supporting the findings of this study are available within the manuscript or are available from the corresponding authors upon request.

CONFLICT OF INTEREST

The authors state no conflict of interest.

ACKNOWLEDGMENTS

We would like to thank Prof. Glenn Morris and the Wolfson Centre for Inherited Neuromuscular Disease for providing us with the MANNES2G antibody, and Iyadh Douagi for assistance with FACS sorting. We would like to acknowledge the MedH Flow Cytometry core facility (Karolinska Institutet), supported by KI/SLL, for providing cell-sorting services. This study was performed in part at the Live Cell Imaging Unit/Nikon Center of Excellence, (Karolinska Institutet). The research was supported by grants to M.E. from the Swedish Research Council and the Center for Innovative Medicine, grants to A.S.C. from Ostermans and Stohnes Foundations and a scholarship to N.V. from Erik and Edith Fernström foundation. A.S.C. could be contacted for specific questions on the experimental procedure, while M.E. could be contacted for general questions on the manuscript content and requests for regents and data files.

AUTHOR CONTRIBUTIONS

Conceptualization: ME, ASC. Formal analysis: ASC, GR, HTH. Funding acquisition: ME, ASC. Investigation: ASC, GR, HTH, DW, RH, JD, PK, DB, FFB, NV.

Methodology: ASC, GR, DW. Project administration: ME. Resources: ME, FFB. Supervision: ME, ASC, NV. Visualization: GR, ASC. Writing – original draft: GR. Writing – review & editing: ME, ASC, GR, HTH, DW, RH, NV.

REFERENCES

Arsenovic PT, Ramachandran I, Bathula K, Zhu R, Narang JD, Noll NA, et al. Nesprin-2G, a Component of the Nuclear LINC Complex, Is Subject to Myosin-Dependent Tension. Biophysical journal 2016;110(1):34-43.

Carrero D, Soria-Valles C, Lopez-Otin C. Hallmarks of progeroid syndromes: lessons from mice and reprogrammed cells. Disease models & mechanisms 2016;9(7):719-35.

Chen CY, Chi YH, Mutalif RA, Starost MF, Myers TG, Anderson SA, et al. Accumulation of the inner nuclear envelope protein Sun1 is pathogenic in progeric and dystrophic laminopathies. Cell 2012;149(3):565-77.

Chen ZJ, Wang WP, Chen YC, Wang JY, Lin WH, Tai LA, et al. Dysregulated interactions between lamin A and SUN1 induce abnormalities in the nuclear envelope and endoplasmic reticulum in progeric laminopathies. J Cell Sci 2014;127(Pt 8):1792-804.

Choi H, Kim TH, Jeong JK, Strandgren C, Eriksson M, Cho ES. Expression of the Hutchinson-Gilford Progeria Mutation Leads to Aberrant Dentin Formation. Sci Rep 2018;8(1):15368.

Choi JY, Lai JK, Xiong ZM, Ren M, Moorer MC, Stains JP, et al. Diminished Canonical beta-Catenin Signaling During Osteoblast Differentiation

Contributes to Osteopenia in Progeria. Journal of bone and mineral research : the official journal of the American Society for Bone and Mineral Research 2018.

Chojnowski A, Ong PF, Wong ES, Lim JS, Mutalif RA, Navasankari R, et al. Progerin reduces LAP2alpha-telomere association in Hutchinson-Gilford progeria. eLife 2015;4.

De Sandre-Giovannoli A, Bernard R, Cau P, Navarro C, Amiel J, Boccaccio I, et al. Lamin a truncation in Hutchinson-Gilford progeria. Science 2003;300(5628):2055.

Dechat T, Pfleghaar K, Sengupta K, Shimi T, Shumaker DK, Solimando L, et al. Nuclear lamins: major factors in the structural organization and function of the nucleus and chromatin. Genes & development 2008;22(7):832-53.

Diamond I, Owolabi T, Marco M, Lam C, Glick A. Conditional gene expression in the epidermis of transgenic mice using the tetracycline-regulated transactivators tTA and rTA linked to the keratin 5 promoter. The Journal of investigative dermatology 2000;115(5):788-94.

Edmondson SR, Thumiger SP, Kaur P, Loh B, Koelmeyer R, Li A, et al. Insulin-like growth factor binding protein-3 (IGFBP-3) localizes to and modulates proliferative epidermal keratinocytes in vivo. The British journal of dermatology 2005;152(2):225-30.

Eriksson M, Brown WT, Gordon LB, Glynn MW, Singer J, Scott L, et al. Recurrent de novo point mutations in lamin A cause Hutchinson-Gilford progeria syndrome. Nature 2003;423(6937):293-8.

Espada J, Varela I, Flores I, Ugalde AP, Cadinanos J, Pendas AM, et al. Nuclear envelope defects cause stem cell dysfunction in premature-aging mice. The Journal of cell biology 2008;181(1):27-35.

Ezhkova E, Pasolli HA, Parker JS, Stokes N, Su IH, Hannon G, et al. Ezh2 orchestrates gene expression for the stepwise differentiation of tissue-specific stem cells. Cell 2009;136(6):1122-35.

Goldman RD, Shumaker DK, Erdos MR, Eriksson M, Goldman AE, Gordon LB, et al. Accumulation of mutant lamin A causes progressive changes in nuclear architecture in Hutchinson-Gilford progeria syndrome. Proceedings of the National Academy of Sciences of the United States of America 2004;101(24):8963-8.

Habib SJ, Chen BC, Tsai FC, Anastassiadis K, Meyer T, Betzig E, et al. A localized Wnt signal orients asymmetric stem cell division in vitro. Science 2013;339(6126):1445-8.

Halaschek-Wiener J, Brooks-Wilson A. Progeria of stem cells: stem cell exhaustion in Hutchinson-Gilford progeria syndrome. J Gerontol A Biol Sci Med Sci 2007;62(1):3-8.

Hernandez L, Roux KJ, Wong ES, Mounkes LC, Mutalif R, Navasankari R, et al. Functional coupling between the extracellular matrix and nuclear lamina by Wnt signaling in progeria. Dev Cell 2010;19(3):413-25.

Horsley V, Aliprantis AO, Polak L, Glimcher LH, Fuchs E. NFATc1 balances quiescence and proliferation of skin stem cells. Cell 2008;132(2):299-310.

Hsu YC, Li L, Fuchs E. Transit-amplifying cells orchestrate stem cell activity and tissue regeneration. Cell 2014;157(4):935-49.

Jaks V, Barker N, Kasper M, van Es JH, Snippert HJ, Clevers H, et al. Lgr5 marks cycling, yet long-lived, hair follicle stem cells. Nat Genet 2008;40(11):1291-9.

Jia HY, Shi Y, Luo LF, Jiang G, Zhou Q, Xu SZ, et al. Asymmetric stem-cell division ensures sustained keratinocyte hyperproliferation in psoriatic skin lesions. Int J Mol Med 2016;37(2):359-68.

Kim PH, Luu J, Heizer P, Tu Y, Weston TA, Chen N, et al. Disrupting the LINC complex in smooth muscle cells reduces aortic disease in a mouse model of Hutchinson-Gilford progeria syndrome. Science translational medicine 2018;10(460).

Kubben N, Voncken JW, Demmers J, Calis C, van Almen G, Pinto Y, et al. Identification of differential protein interactors of lamin A and progerin. Nucleus 2010;1(6):513-25.

Kubben N, Misteli T. Shared molecular and cellular mechanisms of premature ageing and ageing-associated diseases. Nature reviews Molecular cell biology 2017;18(10):595-609.

Lechler T, Fuchs E. Asymmetric cell divisions promote stratification and differentiation of mammalian skin. Nature 2005;437(7056):275-80.

Libotte T, Zaim H, Abraham S, Padmakumar VC, Schneider M, Lu W, et al. Lamin A/C-dependent localization of Nesprin-2, a giant scaffolder at the nuclear envelope. Mol Biol Cell 2005;16(7):3411-24.

Lim X, Tan SH, Koh WL, Chau RM, Yan KS, Kuo CJ, et al. Interfollicular epidermal stem cells self-renew via autocrine Wnt signaling. Science 2013;342(6163):1226-30.

Lombardi ML, Lammerding J. Keeping the LINC: the importance of nucleocytoskeletal coupling in intracellular force transmission and cellular function. Biochem Soc Trans 2011;39(6):1729-34.

Markiewicz E, Tilgner K, Barker N, van de Wetering M, Clevers H, Dorobek M, et al. The inner nuclear membrane protein emerin regulates beta-catenin activity by restricting its accumulation in the nucleus. EMBO J 2006;25(14):3275-85.

Mascre G, Dekoninck S, Drogat B, Youssef KK, Brohee S, Sotiropoulou PA, et al. Distinct contribution of stem and progenitor cells to epidermal maintenance. Nature 2012;489(7415):257-62.

McKenna T, Rosengardten Y, Viceconte N, Baek JH, Grochova D, Eriksson M. Embryonic expression of the common progeroid lamin A splice mutation arrests postnatal skin development. Aging Cell 2014;13(2):292-302.

Mendoza-Reinoso V, Beverdam A. Epidermal YAP activity drives canonical WNT16/beta-catenin signaling to promote keratinocyte proliferation in vitro and in the murine skin. Stem Cell Res 2018;29:15-23.

Merideth MA, Gordon LB, Clauss S, Sachdev V, Smith AC, Perry MB, et al. Phenotype and course of Hutchinson-Gilford progeria syndrome. N Engl J Med 2008;358(6):592-604.

Moore DL, Pilz GA, Arauzo-Bravo MJ, Barral Y, Jessberger S. A mechanism for the segregation of age in mammalian neural stem cells. Science 2015;349(6254):1334-8.

Morris RJ, Liu Y, Marles L, Yang Z, Trempus C, Li S, et al. Capturing and profiling adult hair follicle stem cells. Nat Biotechnol 2004;22(4):411-7.

Neumann S, Schneider M, Daugherty RL, Gottardi CJ, Eming SA, Beijer A, et al. Nesprin-2 interacts with {alpha}-catenin and regulates Wnt signaling at the nuclear envelope. J Biol Chem 2010;285(45):34932-8.

Nowak JA, Polak L, Pasolli HA, Fuchs E. Hair follicle stem cells are specified and function in early skin morphogenesis. Cell Stem Cell 2008;3(1):33-43.

Ouspenskaia T, Matos I, Mertz AF, Fiore VF, Fuchs E. WNT-SHH Antagonism Specifies and Expands Stem Cells prior to Niche Formation. Cell 2016;164(1-2):156-69.

Padmakumar VC, Libotte T, Lu W, Zaim H, Abraham S, Noegel AA, et al. The inner nuclear membrane protein Sun1 mediates the anchorage of Nesprin-2 to the nuclear envelope. J Cell Sci 2005;118(Pt 15):3419-30.

Perdigoto CN, Valdes VJ, Bardot ES, Ezhkova E. Epigenetic regulation of skin: focus on the Polycomb complex. Cellular and molecular life sciences : CMLS 2012;69(13):2161-72.

Porter RM, Lunny DP, Ogden PH, Morley SM, McLean WH, Evans A, et al. K15 expression implies lateral differentiation within stratified epithelial basal cells. Lab Invest 2000;80(11):1701-10.

Posthaus H, Williamson L, Baumann D, Kemler R, Caldelari R, Suter MM, et al. Beta-Catenin is not required for proliferation and differentiation of epidermal mouse keratinocytes. J Cell Sci 2002;115(Pt 23):4587-95.

Prokocimer M, Davidovich M, Nissim-Rafinia M, Wiesel-Motiuk N, Bar DZ, Barkan R, et al. Nuclear lamins: key regulators of nuclear structure and activities. J Cell Mol Med 2009;13(6):1059-85.

Randles KN, Lam le T, Sewry CA, Puckelwartz M, Furling D, Wehnert M, et al. Nesprins, but not sun proteins, switch isoforms at the nuclear envelope during muscle development. Dev Dyn 2010;239(3):998-1009.

Revêchon G, Viceconte N, McKenna T, Sola Carvajal A, Vrtacnik P, Stenvinkel P, et al. Rare progerin-expressing preadipocytes and adipocytes contribute to tissue depletion over time. Sci Rep 2017;7(1):4405.

Rezza A, Wang Z, Sennett R, Qiao W, Wang D, Heitman N, et al. Signaling Networks among Stem Cell Precursors, Transit-Amplifying Progenitors, and their Niche in Developing Hair Follicles. Cell Rep 2016;14(12):3001-18.

Rompolas P, Mesa KR, Kawaguchi K, Park S, Gonzalez D, Brown S, et al. Spatiotemporal coordination of stem cell commitment during epidermal homeostasis. Science 2016;352(6292):1471-4.

Rosengardten Y, McKenna T, Grochova D, Eriksson M. Stem cell depletion in Hutchinson-Gilford progeria syndrome. Aging Cell 2011;10(6):1011-20.

Sada A, Jacob F, Leung E, Wang S, White BS, Shalloway D, et al. Defining the cellular lineage hierarchy in the interfollicular epidermis of adult skin. Nat Cell Biol 2016;18(6):619-31.

Sagelius H, Rosengardten Y, Hanif M, Erdos MR, Rozell B, Collins FS, et al. Targeted transgenic expression of the mutation causing Hutchinson-Gilford progeria syndrome leads to proliferative and degenerative epidermal disease. J Cell Sci 2008;121(Pt 7):969-78.

Salpingidou G, Smertenko A, Hausmanowa-Petrucewicz I, Hussey PJ, Hutchison CJ. A novel role for the nuclear membrane protein emerin in association of the centrosome to the outer nuclear membrane. The Journal of cell biology 2007;178(6):897-904.

Scaffidi P, Misteli T. Lamin A-dependent misregulation of adult stem cells associated with accelerated ageing. Nat Cell Biol 2008;10(4):452-9.

Schmidt E, Nilsson O, Koskela A, Tuukkanen J, Ohlsson C, Rozell B, et al. Expression of the Hutchinson-Gilford progeria mutation during osteoblast development results in loss of osteocytes, irregular mineralization, and poor biomechanical properties. J Biol Chem 2012;287(40):33512-22.

Shumaker DK, Dechat T, Kohlmaier A, Adam SA, Bozovsky MR, Erdos MR, et al. Mutant nuclear lamin A leads to progressive alterations of epigenetic control in premature aging. Proceedings of the National Academy of Sciences of the United States of America 2006;103(23):8703-8.

Sola-Carvajal A, McKenna T, Wallen Arzt E, Eriksson M. Overexpression of Lamin B Receptor Results in Impaired Skin Differentiation. PLoS One 2015;10(6):e0128917.

Strandgren C, Revêchon G, Sola-Carvajal A, Eriksson M. Emerging candidate treatment strategies for Hutchinson-Gilford progeria syndrome. Biochem Soc Trans 2017;45(6):1279-93.

Supek F, Bošnjak M, Škunca N, Šmuc T. REVIGO summarizes and visualizes long lists of gene ontology terms. PLoS One 2011;6(7):e21800.

Trapnell C, Pachter L, Salzberg SL. TopHat: discovering splice junctions with RNA-Seq. Bioinformatics 2009;25(9):1105-11.

Trapnell C, Roberts A, Goff L, Pertea G, Kim D, Kelley DR, et al. Differential gene and transcript expression analysis of RNA-seq experiments with TopHat and Cufflinks. Nat Protoc 2012;7(3):562-78.

Tripp CS, Blomme EA, Chinn KS, Hardy MM, LaCelle P, Pentland AP. Epidermal COX-2 induction following ultraviolet irradiation: suggested mechanism for

the role of COX-2 inhibition in photoprotection. The Journal of investigative dermatology 2003;121(4):853-61.

Troy TC, Arabzadeh A, Turksen K. Re-assessing K15 as an epidermal stem cell marker. Stem Cell Rev 2011;7(4):927-34.

Vaughan A, Alvarez-Reyes M, Bridger JM, Broers JL, Ramaekers FC, Wehnert M, et al. Both emerin and lamin C depend on lamin A for localization at the nuclear envelope. J Cell Sci 2001;114(Pt 14):2577-90.

Wang J, Duncan D, Shi Z, Zhang B. WEB-based GEne SeT AnaLysis Toolkit (WebGestalt): update 2013. Nucleic Acids Res 2013;41(Web Server issue):W77-83.

Wang J, Vasaikar S, Shi Z, Greer M, Zhang B. WebGestalt 2017: a more comprehensive, powerful, flexible and interactive gene set enrichment analysis toolkit. Nucleic Acids Res 2017;45(W1):W130-W7.

Waseem A, Dogan B, Tidman N, Alam Y, Purkis P, Jackson S, et al. Keratin 15 expression in stratified epithelia: downregulation in activated keratinocytes. The Journal of investigative dermatology 1999;112(3):362-9.

Zhang B, Kirov S, Snoddy J. WebGestalt: an integrated system for exploring gene sets in various biological contexts. Nucleic Acids Res 2005;33(Web Server issue):W741-8.

Zhang Q, Ragnauth CD, Skepper JN, Worth NF, Warren DT, Roberts RG, et al. Nesprin-2 is a multi-isomeric protein that binds lamin and emerin at the nuclear envelope and forms a subcellular network in skeletal muscle. J Cell Sci 2005;118(Pt 4):673-87.

FIGURE LEGENDS

Figure 1. Imbalance in division orientation in HGPS IFE stem cells.

(a) Immunofluorescent staining of skin tissues showing cells dividing either parallel or perpendicular to the basement membrane (white dots). The mitotic spindles were visible after tubulin staining in basal cells. Analysis of the cell division orientation was done for E18.5 **(b)** and PD4 **(c)** HGPS and wild-type mice IFE. A minimum of 40 dividing cells from 3 different animals were analyzed based on their degree of division orientation relative to the basement membrane. **(d)** Graph representing the percentage of mitotic cells according to the division orientation at E18.5 and PD4 HGPS and wild-type mice. Scale bars: (a) = 10μm.

Figure 2. HGPS skin is marked by increased proliferation.

(a) Heatmap comparison of proliferation and quiescence gene signatures (GS) with the RNA sequencing data, showing up- and downregulated genes represented as –log10(p-value) **(b)** PHH3 immunohistochemistry in skin from PD4 HGPS and wild-type mice. Quantification of positive cells in the IFE **(c)** and HF **(d)** (n = 3/group). Data are represented as mean ± SEM. Scale bars: (b) = 50μm.

Figure 3. Loss of nuclear β-catenin in HGPS.

(a) β-catenin and progerin immunofluorescent co-staining in control and HGPS fibroblasts. **(b)** Nuclear β-catenin fluorescence intensity quantification from early and late passage fibroblasts (early passage > 192cells/group; late passage > 36cells/group). Boxplots represent min, median and max. **(c)** β-catenin and progerin immunofluorescent co-staining in PD4 HGPS and wild-type IFE. **(d)** Nuclear β-

catenin fluorescence intensity quantification (n = 3/group). Data are represented as mean ± SEM. Scale bars: (c) = 20μm, (e) = 10μm.

Figure 4. Progerin expression results in emerin accumulation at the nuclear periphery

(a-b) Emerin levels were determined by immunofluorescent staining (a) and subsequently measured as fluorescence intensity in cell nuclei (b) from wild-type, HGPS and Lamin A overexpressing mice IFE at E18.5, PD4 and PD28. **(c)** Intensity profiles were generated to determine the localization of emerin accumulation in wild-type, HGPS and lamin A overexpressing keratinocytes. Micrographs of emerin in cell nuclei show examples of how the intensity profiles were created. Data are represented as mean ± SEM. Scale bars: (a) = 10μm.

Figure 5. Nesprin-2 is reduced at the nuclear rim in HGPS fibroblasts.

(a) Nesprin-2 protein levels were established by immunofluorescent staining in control and HGPS patient fibroblasts. **(b)** Nuclear and perinuclear fluorescence intensities were assessed in control and patients fibroblasts at both early and late passages. Data are represented as mean ± SEM. Scale bars: (a) = 50μm.

ACCEPTED MANUSCRIPT

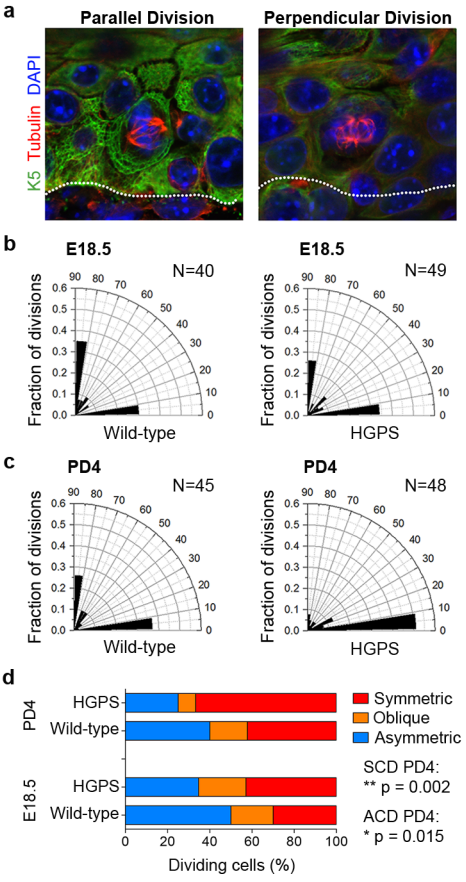

ACCEPTED MANUSCRIPT

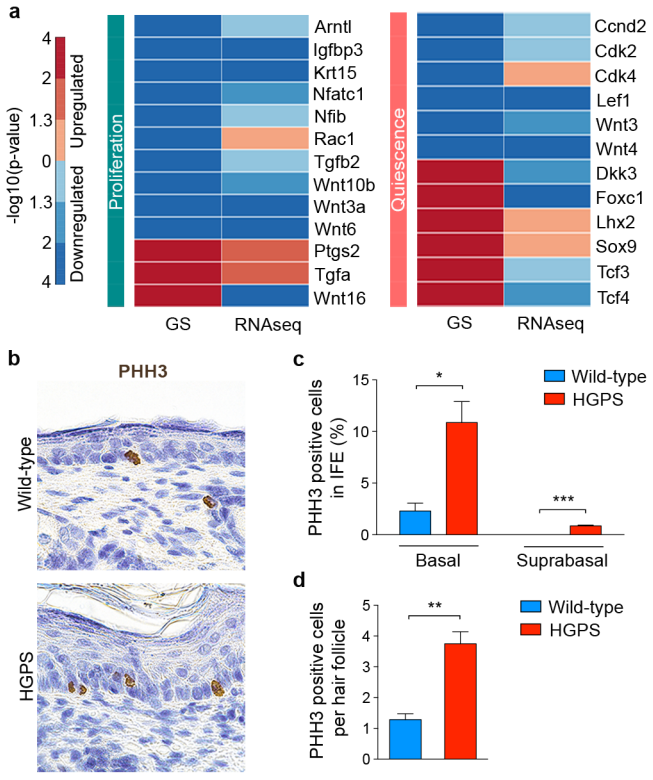

ACCEPTED MANUSCRIPT

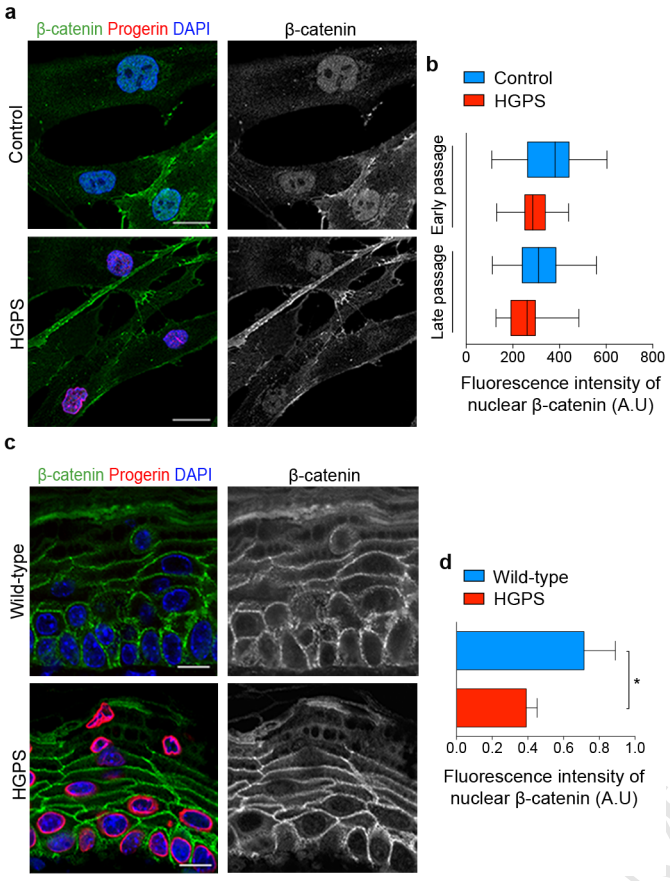

ACCEPTED MANUSCRIPT

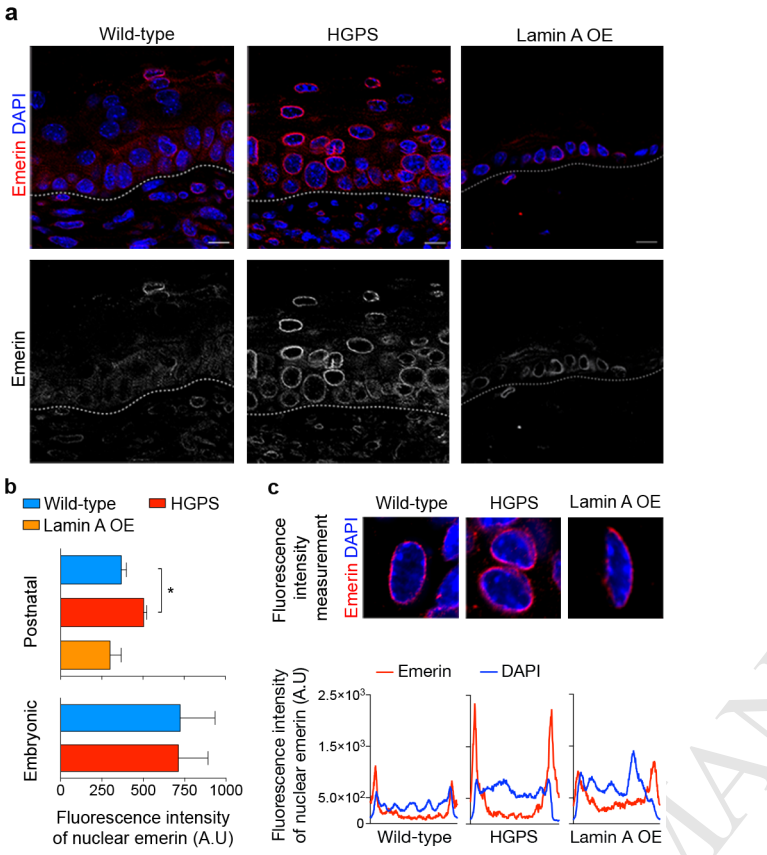

ACCEPTED MANUSCRIPT

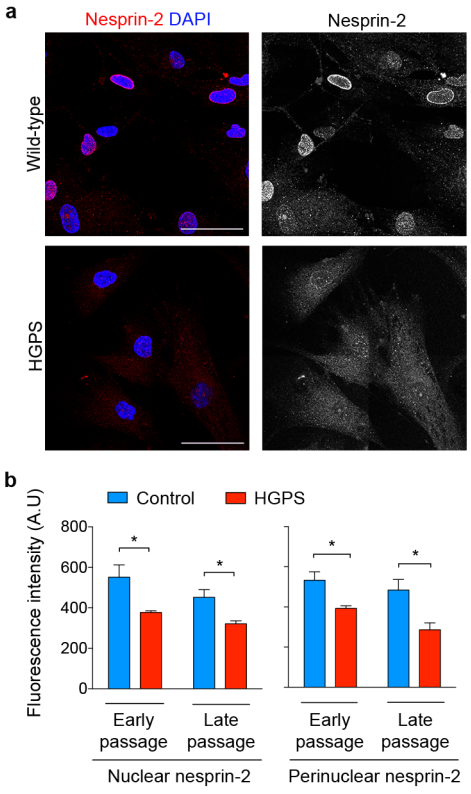

ACCEPTED MANUSCRIPT

ACCEPTED MANUSCRIPT

SUPPLEMENTARY METHODS

Transgenic mice

Animal studies were approved by the Stockholm South Ethical review board (Dnr. 35-15). All procedures were performed in accordance with the institutional guidelines and regulations. Transgenic mice were housed under a 12-hour light/dark cycle, at 20–22°C and 50–60% humidity in a pathogen-free animal facility within Karolinska University Hospital, Huddinge, Sweden. Heterozygous tetop-LA^{G608G} or tetop-LA^{wt} (Sagelius et al., 2008) mice were intercrossed with heterozygous K5-tTA mice (Diamond et al., 2000), and offsprings were genotyped in accordance with previously described procedures (McKenna et al., 2014, Sagelius et al., 2008). Throughout the paper, tetop-LA^{G608G+}; K5-tTA^{+} bitransgenic mice are referred to as HGPS. Non-transgenic littermates were used as control mice and are referred to as wild-type.

Tissue collection and processing

Animals were sacrificed by an excess of isoflurane. Minimum 3 mice per group were used in each experiment and analysis. Dorsal skin was collected and fixed in 4% paraformaldehyde (pH 7.4) at 4°C overnight. Samples were dehydrated and embedded in paraffin. Four-micrometer thick sections were used for immunofluorescence analysis. For quantification of cell division orientation ten-micrometer thick sections were used and every second section was collected to avoid duplicates during analysis.

Tissue immunostaining

Tissue immunostainings were done as previously described (Revêchon et al., 2017). The following primary antibodies were used: anti-keratin 5 (1:500, PRB-160P; BioSite, San Diego, CA, USA), anti-alpha tubulin (1:500, Abcam), anti-beta catenin (1:100, CAT-15, ThermoFisher Scientific), anti-progerin (1:150, mAb 134A, Enzo Life Science), anti-emerin (1:40, NCL-Emerin, Leica) and anti-phospho-Histone H3 (1:350, Ser 10, Millipore).

Image acquisition and analysis

Immunofluorescence imaging was performed using Nikon A1R and A1+ imaging systems (Nikon corporation, Japan), and images were analyzed with NIS elements (Nikon Corporation, Japan). To determine the symmetry of cell division, cells presenting a division angle between 0-30º towards the basement membrane were considered as dividing parallel, cells with a division of 30°-60° were considered as oblique, and cells with a division angle between 60-90º were considered as dividing perpendicular. Immunohistochemical imaging was done using the Zeiss Axioplan 2 microscope (Carl Zeiss AG, Germany) coupled to the Zeiss Axiocam MRm camera. Images were analyzed with the Image-Pro Insight 9.1 software.

Keratinocyte isolation and FACS

Primary keratinocytes were isolated and processed for FACS as previously described (Rosengardten et al., 2011). Single-cell suspensions of isolated keratinocytes were incubated for 30 min with PE-Cy5-conjugated anti-α6-integrin (1:5, CD49f; BD biosciences) and APC-conjugated anti-CD45 (1:40; 30-F11; BD biosciences) antibodies. Samples were sorted into basal (CD45^{neg}/CD49f^{high}) and suprabasal (CD45^{neg}/CD49f^{low}) populations in SMEM media using a FACScalibur flow cytometer (BD biosciences, USA).

Keratinocytes subpopulations RNA sequencing

After sorting, cells were pelleted by centrifugation and re-suspended in Trizol (Invitrogen) followed by chloroform extraction. The aqueous phase was applied to RNeasy minElute column (Qiagen) and the RNA was purified according to manufacturer instructions. Total RNA was subjected to quality control with Agilent Bioanalyser according to the manufacturer's instructions. To construct libraries suitable for Illumina sequencing, the Nugen Ovation RNA Seq Systems (cat: 0348-32) for model organisms was used. The protocol enables preparation of strand-specific RNA-seq libraries from small amounts of total RNA. 10 ng RNA/sample was subjected to cDNA synthesis, ligation of adapters and amplification of indexed libraries. The yield and quality of the amplified libraries was analysed using Qubit (Thermo Fisher) and the Agilent Tapestation. The indexed cDNA libraries were normalised and combined and the pools were sequenced on the Illumina HiSeq 2000 for a 200-cycle v3 sequencing run generating 100 bp paired-end reads. Base calling and demultiplexing was performed using CASAVA software with default settings generating Fastq files. The generated sequence reads were mapped to the mouse genome (mm10) using Galaxy software. Sequences were aligned to the reference genome using TopHat (Trapnell et al., 2009) and differential expression analysis was done using Cufflinks (Trapnell et al., 2012).

Gene enrichment analysis

Differentially expressed genes were analyzed for gene set enrichment of GO functions and Wikipathway using Webgestalt (Wang et al., 2013, Wang et al., 2017, Zhang B. et al., 2005). We used a hypergeometric statistical test, and Benjamini-Hochberg procedure as multiple test adjustment of p-values. Due to a small dataset, analysis was carried out on genes with a FDR < 0.1. GO terms were plotted using

ACCEPTED MANUSCRIPT

REVIGO (Supek et al., 2011).

Expression array

Scanning of arrays was performed using an Affymetrix GeneChip Scanner 3000 7G, and the generated image files were preprocessed using the Affymetrix GeneChip Command Console (AGCC, v.3.2) software to generate cell intensity (CEL) files. The CEL files were imported to the Affymetrix Expression Console (EC, v.1.2) software and analyzed using the Robust Multichip Average (RMA) method including quantile normalization and median polish summarization. EC quality assessment metrics were within boundaries for all samples.

***In situ* hybridization**

K15 transcripts were detected using RNAscope (Advanced Cell Diagnostic) in accordance with the manufacturer's protocol. Few modifications were made: target retrieval was performed for 20 minutes and Protease Plus was applied for 30 minutes. RNAscope assay was followed by addition of anti-keratin5 antibody. Analysis was done using NIS elements software.

Cell culture and immunofluorescence

HGPS and unaffected primary dermal fibroblasts were obtained from the Coriell Cell Repositories (Camden, NJ, USA). Cells were grown in a monolayer in T25 flasks (Sarstedt) in a humidified 37°C 5% CO2 incubator. Growth medium consisted of DMEM (Gibco) supplemented with 15% fetal bovine serum (Biowest), and 1X L-glutamine and 1X penicillin–streptomycin (Gibco). For immunofluorescence cells were grown in glass-bottom dishes (Matek) and fixed in 4% PFA for 10 minutes at room temperature. After permeabilization with 1% NP-40 and blocking with normal goat serum, cell were incubated overnight at 4ºC with the following primary antibodies: anti-beta catenin (1:100, CAT-15, Invitrogen), anti-progerin (1:150, mAb 134A, Enzo) and anti-active beta catenin (1:100, 8E7, Merck Millipore), and anti-nesprin-2 MANNES2G (1:50, 4B5, Randles et al., 2010). Secondary antibody incubations were done with Alexa 488-conjugated goat anti-rabbit (1:1000, A-11008, Life Technologies) and Alexa 555-conjugated goat anti-mouse (1:1000, A-28180, Life Technologies). (Active) nuclear β-catenin and (peri-)nuclear nesprin-2 intensity were measured using NIS elements software. Nuclear β-catenin intensity was measured in IFE keratinocytes by marking of the nuclear area (as determined by DAPI staining) and by measuring the average fluorescence intensity across the whole nucleus. Intensity values were normalized to DAPI intensity levels, to reduce potential spectral bleed-through artifacts.

Wnt3a stimulation

70% confluent cell cultures were stimulated with 150 ng/ml of mouse recombinant Wnt3a (Peprotech) for a time course of 8, 16 or 24 hours. After stimulation cells were processed for immunofluorescence as described above, for mRNA expression or western blot analysis as previously described (Sola-Carvajal et al., 2015).

Statistical analysis

Statistical analyses were performed using unpaired Student's t-tests with a two-tailed 95% confidence interval. Statistical analysis of ACD quantification was performed using Fisher's exact test with Bonferroni adjustments. Significance was defined as $p < 0.05$ (*$p < 0.05$; **$p < 0.005$). Values are represented as mean ± SEM.

SUPPLEMENTARY REFERENCES

Augustin I, Gross J, Baumann D, Korn C, Kerr G, Grigoryan T, et al. Loss of epidermal Evi/Wls results in a phenotype resembling psoriasiform dermatitis. The Journal of experimental medicine 2013;210(9):1761-77.

Benitah SA, Frye M, Glogauer M, Watt FM. Stem cell depletion through epidermal deletion of Rac1. Science 2005;309(5736):933-5.

Chang CY, Pasolli HA, Giannopoulou EG, Guasch G, Gronostajski RM, Elemento O, et al. NFIB is a governor of epithelial-melanocyte stem cell behaviour in a shared niche. Nature 2013;495(7439):98-102.

Geyfman M, Kumar V, Liu Q, Ruiz R, Gordon W, Espitia F, et al. Brain and muscle Arnt-like protein-1 (BMAL1) controls circadian cell proliferation and susceptibility to UVB-induced DNA damage in the epidermis. Proceedings of the National Academy of Sciences of the United States of America 2012;109(29):11758-63.

Nguyen H, Merrill BJ, Polak L, Nikolova M, Rendl M, Shaver TM, et al. Tcf3 and Tcf4 are essential for long-term homeostasis of skin epithelia. Nat Genet 2009;41(10):1068-75.

Oshimori N, Fuchs E. Paracrine TGF-beta signaling counterbalances BMP-mediated repression in hair follicle stem cell activation. Cell Stem Cell 2012;10(1):63-75.

Rhee H, Polak L, Fuchs E. Lhx2 maintains stem cell character in hair follicles. Science 2006;312(5782):1946-9.

Tripp CS, Blomme EA, Chinn KS, Hardy MM, LaCelle P, Pentland AP. Epidermal COX-2 induction following ultraviolet irradiation: suggested mechanism for the role of COX-2 inhibition in photoprotection. The Journal of investigative dermatology 2003;121(4):853-61.

Vassar R, Fuchs E. Transgenic mice provide new insights into the role of TGF-alpha during epidermal development and differentiation. Genes & development 1991;5(5):714-27.

Wang L, Siegenthaler JA, Dowell RD, Yi R. Foxc1 reinforces quiescence in self-renewing hair follicle stem cells. Science 2016;351(6273):613-7.

Yang H, Adam RC, Ge Y, Hua ZL, Fuchs E. Epithelial-Mesenchymal Micro-niches Govern Stem Cell Lineage Choices. Cell 2017;169(3):483-96 e13.

Table S1. Top 50 GO enrichment analysis of DEG in keratinocytes[1]

ACCEPTED MANUSCRIPT

BASAL				
Category[2]	**p-value**	**FDR**	**Genes (No.)**	**Genes on list (%)**
Tissue development	0	0	66	21,4
Enzyme linked receptor protein signaling pathway	2,85E-13	1,19E-09	38	12,3
Epithelium development	2,39E-12	6,64E-09	43	14,0
Regulation of cell differentiation	6,13E-12	1,28E-08	52	16,9
Ossification	1,71E-11	2,85E-08	24	7,8
Negative regulation of developmental process	1,77E-10	2,45E-07	35	11,4
Epidermis development	1,35E-09	1,61E-06	19	6,2
Response to endogenous stimulus	2,45E-09	2,30E-06	44	14,3
Cellular response to endogenous stimulus	2,76E-09	2,30E-06	37	12,0
Circulatory system development	2,77E-09	2,30E-06	35	11,4
Cell death	9,52E-09	6,34E-06	50	16,2
Skin development	1,03E-08	6,34E-06	17	5,5
Negative regulation of multicellular organismal process	1,03E-08	6,34E-06	35	11,4
Transmembrane receptor protein tyrosine kinase signaling pathway	1,07E-08	6,34E-06	24	7,8
Cellular response to organic substance	1,59E-08	8,65E-06	51	16,6
Response to oxygen-containing compound	1,87E-08	8,65E-06	42	13,6
Regulation of catalytic activity	1,88E-08	8,65E-06	53	17,2
Regulation of multicellular organismal development	1,95E-08	8,65E-06	47	15,3
Negative regulation of cell differentiation	2,04E-08	8,65E-06	27	8,8
Osteoblast differentiation	2,17E-08	8,65E-06	15	4,9
Neurogenesis	2,18E-08	8,65E-06	43	14,0
Muscle structure development	3,11E-08	1,18E-05	25	8,1
Cell adhesion	3,77E-08	1,37E-05	44	14,3
Cellular response to oxygen-containing compound	3,96E-08	1,38E-05	31	10,1
Blood vessel development	4,23E-08	1,41E-05	25	8,1
Biological adhesion	4,57E-08	1,47E-05	44	14,3
Single organism cell adhesion	5,81E-08	1,79E-05	28	9,1
Regulation of transcription from RNA polymerase II promoter	6,58E-08	1,91E-05	47	15,3
Transcription from RNA Polymerase II promoter	6,67E-08	1,91E-05	48	15,6
Locomotion	6,87E-08	1,91E-05	42	13,6
Programmed cell death	7,70E-08	2,07E-05	46	14,9
Regulation of growth	8,15E-08	2,12E-05	25	8,1
Anatomical structure formation involved in morphogenesis	8,55E-08	2,16E-05	33	10,7
Vasculature development	9,56E-08	2,34E-05	25	8,1
Apoptotic process	1,36E-07	3,23E-05	45	14,6
Cardiovascular system development	1,48E-07	3,43E-05	25	8,1
Positive regulation of RNA metabolic process	1,71E-07	3,85E-05	39	12,7
Epithelial cell differentiation	1,76E-07	3,85E-05	24	7,8
Positive regulation of biosynthetic process	2,64E-07	5,65E-05	44	14,3
Positive regulation of nucleobase-containing compound metabolic process	4,30E-07	8,95E-05	42	13,6
Growth	4,95E-07	1,01E-04	31	10,1
Cell migration	5,42E-07	1,07E-04	34	11,0
Positive regulation of catalytic activity	6,22E-07	1,15E-04	36	11,7
Protein phosphorylation	7,51E-07	1,31E-04	43	14,0
Cell motility	7,56E-07	1,31E-04	36	11,7
Localization of cell	7,56E-07	1,31E-04	36	11,7
Positive regulation of nitrogen compound metabolic process	7,89E-07	1,34E-04	43	14,0
Positive regulation of macromolecule biosynthetic process	1,23E-06	2,05E-04	40	13,0
Response to growth factor	1,27E-06	2,06E-04	22	7,1
Response to external stimulus	1,32E-06	2,06E-04	47	15,3

SUPRABASAL				
Category[2]	**p-value**	**FDR**	**Genes (No.)**	**Genes on list (%)**
Tissue development	1,30E-10	5,42E-07	24	29,3
Epithelium development	1,96E-08	4,08E-05	17	20,7
Regulation of cell differentiation	6,91E-07	5,75E-04	18	22,0
Response to endogenous stimulus	3,98E-06	2,07E-03	16	19,5
Cellular response to organic substance	1,05E-05	4,59E-03	18	22,0
Cell death	2,27E-05	7,91E-03	17	20,7
Regulation of cell death	2,29E-05	7,91E-03	15	18,3
Positive regulation of gene expression	7,77E-05	1,62E-02	15	18,3
Regulation of catalytic activity	9,40E-05	1,66E-02	17	20,7
Positive regulation of biosynthetic process	1,17E-04	1,82E-02	15	18,3
Apoptotic process	1,33E-04	1,99E-02	15	18,3
Programmed cell death	1,56E-04	2,10E-02	15	18,3
Cell development	2,26E-04	2,51E-02	16	19,5
Cell proliferation	2,58E-04	2,68E-02	15	18,3

[1]DEG selection criterion: FDR < 0.1, [2]Inclusion criteria: p-value < 0.05, FDR < 0.1 and No. Genes > 15.
Total number of basal genes: 308; total number of suprabasal genes: 82.

Table S2. Stemness gene expression in keratinocytes

ACCEPTED MANUSCRIPT

			BASAL					
			RNA sequencing			Array		
Localization	**Stem cell lineage**	**Gene**	**log$_2$(FC)**	**p-value**	**FDR**	**log$_2$(FC)**	**p-value**	**FDR**
IFE	**LRC**	Adam8	-0,7396	3,75E-02	3,21E-01	-1,1885	2,78E-02	3,71E-01
		Adrb1	-1,8518	7,80E-03	9,48E-02	-1,2484	3,27E-01	4,85E-01
		Ankrd24	-1,9041	1,33E-02	1,40E-01	1,0400	5,79E-01	5,76E-01
		Antxr1	-1,0059	6,50E-04	3,71E-02	-1,9300	1,13E-01	3,96E-01
		Col6a1	-4,5935	7,90E-03	9,48E-02	-1,1006	6,09E-01	5,86E-01
		Igfbp3	-3,2211	5,00E-05	8,58E-03	-2,8140	2,40E-01	4,47E-01
		Ipo7	0,6241	2,52E-02	2,40E-01	1,0491	7,15E-01	6,16E-01
		Npr3	-2,8565	1,78E-02	1,80E-01	-1,4176	2,66E-01	4,59E-01
		Nr2c1	-0,9381	1,96E-02	1,95E-01	-1,1950	9,29E-02	3,84E-01
		Ptgs2	0,7089	1,24E-02	1,32E-01	1,1495	2,68E-01	4,60E-01
		Slc6a4	-1,7626	2,11E-02	2,08E-01	-1,3450	1,29E-01	4,00E-01
		Sox6	-1,4525	3,60E-03	4,99E-02	-1,8437	1,49E-01	4,09E-01
		Tmsb10	-0,7714	3,33E-02	2,95E-01	-1,0266	5,01E-01	5,51E-01
		Wnt6	-1,4232	6,50E-04	3,71E-02	-1,1377	4,29E-01	5,25E-01
	nLRC	C1qtnf1	-5,8710	5,00E-05	8,58E-03	-1,2241	2,27E-01	4,42E-01
		Fn1	-0,6380	2,61E-02	2,45E-01	-1,4009	1,41E-01	4,06E-01
		Slc1a3	-0,9749	8,35E-03	9,48E-02	-1,4522	1,15E-01	3,96E-01
		Trp73	-0,6521	4,55E-02	3,67E-01	-1,1665	2,38E-02	3,71E-01
HF	**HFSC**	Arhgef19	-1,6817	9,65E-03	1,06E-01	-1,1868	2,51E-01	4,52E-01
		Atp6v1b1	-1,3973	1,51E-02	1,55E-01	-2,1833	1,44E-01	4,08E-01
		Ccl20	1,6641	3,50E-04	3,71E-02	2,7402	8,96E-02	3,84E-01
		Cgnl1	-1,9760	1,58E-02	1,62E-01	1,1024	2,22E-01	4,40E-01
		Crim1	-0,6800	1,21E-02	1,28E-01	-1,3060	6,28E-03	3,58E-01
		Ctgf	-1,1461	1,19E-02	1,27E-01	-1,0538	6,61E-01	6,01E-01
		Dlk2	-1,1394	4,50E-02	3,64E-01	-1,1648	3,48E-02	3,71E-01
		Egr2	-0,8616	2,17E-02	2,12E-01	-1,1583	4,35E-01	5,27E-01
		Fam101b	-1,0907	3,39E-02	2,98E-01	-1,1485	1,10E-01	3,94E-01
		Fam110c	-1,3591	2,79E-02	2,58E-01	-1,7652	1,83E-01	4,25E-01
		Foxc1	-1,4259	3,50E-03	4,86E-02	-1,0405	5,55E-01	5,69E-01
		Fzd7	-0,8184	1,08E-02	1,17E-01	1,0441	5,31E-01	5,61E-01
		Fzd8	-2,1543	1,45E-02	1,50E-01	-1,4332	1,05E-02	3,59E-01
		Gas1	-1,7253	5,00E-05	8,58E-03	-1,2659	2,97E-03	3,56E-01
		Il15ra	1,1224	3,79E-02	3,24E-01	1,1771	1,84E-01	4,25E-01
		Il33	0,6477	4,10E-02	3,42E-01	-1,0041	9,80E-01	6,82E-01
		Krt15	-2,3797	8,00E-04	3,71E-02	-1,7350	1,89E-01	4,27E-01
		Man1c1	-1,6534	2,00E-02	1,99E-01	-2,0194	1,29E-01	4,00E-01
		Nfatc1	-0,5861	3,92E-02	3,31E-01	-1,0229	8,62E-01	6,54E-01
		Osgin1	1,2274	4,40E-02	3,58E-01	1,0364	5,69E-01	5,73E-01
		Pdk4	-2,0112	1,81E-02	1,82E-01	-1,3404	3,42E-01	4,92E-01
		Slc1a3	-0,9749	8,35E-03	9,48E-02	-1,4522	1,15E-01	3,96E-01
		Tox	-1,7054	4,32E-02	3,53E-01	-1,0463	5,33E-01	5,62E-01
	TAC	Foxq1	-2,7031	8,70E-03	9,64E-02	-1,3120	2,90E-01	4,69E-01
		Id1	-1,1881	1,50E-04	1,89E-02	-1,4665	1,91E-01	4,28E-01
		Ivl	1,1673	1,10E-02	1,18E-01	1,5927	5,11E-01	5,54E-01
		Lef1	-2,0656	5,00E-05	8,58E-03	-1,9617	1,87E-01	4,26E-01
		Lzts1	2,0340	1,55E-03	3,71E-02	1,2170	3,18E-01	4,80E-01
		Nckap5	-1,4549	5,00E-03	6,62E-02	-1,3339	2,16E-01	4,38E-01
		Odc1	-1,2153	5,60E-03	7,35E-02	-1,1167	6,19E-01	5,89E-01
		Tob1	-0,8266	6,50E-03	8,43E-02	-1,3787	4,67E-02	3,72E-01
		Trpv3	0,6989	5,00E-02	3,93E-01	1,3934	1,30E-02	3,61E-01

			SUPRABASAL					
			RNA sequencing			Array		
Localization	**Stem cell lineage**	**Gene**	**log$_2$(FC)**	**p-value**	**FDR**	**log$_2$(FC)**	**p-value**	**FDR**
IFE	**LRC**	Abcg4	2,3345	9,80E-03	1,83E-01	1,0423	4,67E-01	7,63E-01
		Acsl1	-0,7251	4,42E-02	4,85E-01	-1,4264	2,93E-01	7,18E-01
		Alox12	-1,9345	1,50E-03	1,40E-01	-1,8519	2,61E-01	7,08E-01
		Ankrd35	-1,4825	4,50E-04	5,95E-02	-1,0861	6,21E-01	7,93E-01
		Cobl	-1,1895	1,24E-02	2,15E-01	-1,2139	2,96E-01	7,18E-01
		Hspa12a	-3,9163	1,38E-02	2,32E-01	-1,4601	1,16E-01	6,69E-01
		Mt4	-2,5770	4,78E-02	5,06E-01	-1,4741	9,75E-02	6,60E-01
		Npl	-1,8651	5,00E-05	1,61E-02	-2,1172	2,40E-01	7,02E-01
		Serpinb12	-2,1697	3,00E-04	4,53E-02	-2,8927	3,10E-01	7,21E-01
		Them5	-1,2583	1,70E-03	1,41E-01	-1,5848	4,05E-01	7,46E-01
		Tmem246	-3,1306	1,06E-02	1,94E-01	-1,1814	1,37E-01	6,77E-01
		Trim2	-1,2004	1,08E-02	1,96E-01	-1,0918	1,56E-01	6,80E-01
	nLRC	Ddah1	0,8640	4,66E-02	5,00E-01	1,2686	7,46E-01	8,15E-01
		Gyk	1,0097	3,81E-02	4,46E-01	2,0172	1,54E-01	6,80E-01
		Knstrn	-1,0665	4,36E-02	4,82E-01	1,0844	6,09E-01	7,91E-01
		Rassf10	-1,2595	7,30E-03	1,56E-01	-1,0741	5,35E-01	7,76E-01
		Slc1a3	-1,3593	2,86E-02	3,81E-01	-1,1992	5,36E-01	7,76E-01

Table S3. Quiescence and proliferation in basal keratinocytes

ACCEPTED MANUSCRIPT

	Literature				RNA sequencing	
Gene	**Regulation**	**Localization**	**Function**	**Reference**	**log_2(FC)***	**p-value**
Arntl	Down	Epidermis	Proliferation	Geyfman et al., 2012	-0,3440	2,96E-01
Igfbp3	Down	IFE	Proliferation	Edmondson et al., 2005	-3,2211	5,00E-05
Krt15	Down	Epidermis	Proliferation	Augustin et al., 2013	-2,3797	8,00E-04
Nfatc1	Down	HF	Proliferation	Horsley et al., 2008	-0,5861	3,92E-02
Nfib	Down	HF	Proliferation	Chang et al., 2013	-0,1240	6,92E-01
Rac1	Down	Epidermis	Proliferation	Benitah et al., 2005	0,2172	4,13E-01
Tgfb2	Down	HF	Proliferation	Oshimori and Fuchs, 2012	-0,0743	8,64E-01
Wnt10b	Down	Skin	Proliferation	Mendoza et al., 2018	-1,0441	1,51E-02
Wnt3a	Down	Skin	Proliferation	Mendoza et al., 2018	-1,7523	1,00E-04
Wnt6	Down	Skin	Proliferation	Mendoza et al., 2018	-1,4232	6,50E-04
Ptgs2	Up	IFE	Proliferation	Tripp et al., 2003	0,7089	1,24E-02
Tgfa	Up	IFE	Proliferation	Vassar and Fuchs, 1991	0,7671	3,61E-02
Wnt16	Up	Skin	Proliferation	Mendoza et al., 2018	-2,4294	5,00E-05
Ccnd2	Down	HF	Quiescence	Yang et al., 2017	-0,0711	8,27E-01
Cdk2	Down	HF	Quiescence	Yang et al., 2017	-0,2898	3,69E-01
Cdk4	Down	HF	Quiescence	Yang et al., 2017	0,0157	9,61E-01
Lef1	Down	HF	Quiescence	Yang et al., 2017	-2,0656	5,00E-05
Wnt3	Down	HF	Quiescence	Yang et al., 2017	-0,6346	2,01E-02
Wnt4	Down	HF	Quiescence	Yang et al., 2017	-0,8524	4,15E-03
Dkk3	Up	HF	Quiescence	Yang et al., 2017	-1,1918	3,18E-02
Foxc1	Up	HF	Quiescence	Wang et al., 2016	-1,4259	3,50E-03
Lhx2	Up	HF	Quiescence	Rhee et al., 2006	0,1127	8,31E-01
Sox9	Up	HF	Quiescence	Nowak et al., 2008	0,2597	3,25E-01
Tcf3	Up	HF	Quiescence	Nguyen et al., 2009	-0,3294	2,56E-01
Tcf4	Up	HF	Quiescence	Nguyen et al., 2009	-0,8678	1,98E-02

* log2(FC): log2(fold change)
IFE: Interfollicular epidermis
HF: Hair follicle

ACCEPTED MANUSCRIPT

Table S4. Wikipathway analysis of differentially expressed genes in keratinocytes[1]

ACCEPTED MANUSCRIPT

BASAL				
Pathway[2]	**p-value**	**FDR**	**Genes (No.)**	**Genes**
Wnt Signaling in Kidney Disease	9,12E-06	1,56E-03	7	Fzd5; Wnt3a; Wnt4; Wnt6; Wnt7b; Fzd2; Wnt16
ESC Pluripotency Pathways	1,61E-04	1,31E-02	10	Fos; Fzd5; Gab1; Pdgfb; Wnt3a; Wnt4; Wnt6; Wnt7b; Fzd2; Wnt16
Wnt Signaling Pathway	2,30E-04	1,31E-02	7	Fzd5; Wnt3a; Wnt4; Wnt6; Wnt7b; Fzd2; Wnt16
Factors and pathways affecting IGF1-Akt signaling	4,13E-04	1,76E-02	5	Igfbp3; Igfbp5; Irs1; Tnf; Foxo1
Wnt Signaling Pathway and Pluripotency	9,00E-04	3,08E-02	8	Fzd5; Lef1; Wnt3a; Wnt4; Wnt6; Wnt7b; Fzd2; Wnt16
Spinal Cord Injury	4,30E-03	1,23E-01	7	Rhob; Cspg4; Btg2; Vcan; Egr1; Fos; Tnf
Adipogenesis genes	6,86E-03	1,67E-01	8	Socs3; Cntfr; Id3; Irs1; Mef2a; Tnf; Klf6; Foxo1
IL-7 Signaling Pathway	1,32E-02	2,53E-01	4	Irf1; Irs1; Pik3r1; Foxo1
IL-9 Signaling Pathway	1,33E-02	2,53E-01	3	Socs3; Irs1; Pik3r1
IL-6 signaling Pathway	1,74E-02	2,60E-01	6	Socs3; Fos; Gab1; Pik3r1; Ppp2r5b; Foxo1
Insulin Signaling	1,82E-02	2,60E-01	8	Socs3; Egr1; Fos; Gab1; Irs1; Pik3r1; Tbc1d4; Foxo1
IL-3 Signaling Pathway	1,82E-02	2,60E-01	6	Cish; Socs3; Gab1; Id1; Pik3r1; Foxo1
Oxidative Stress	2,03E-02	2,67E-01	3	Fos; Junb; Mt1
TGF Beta Signaling Pathway	2,32E-02	2,83E-01	4	Fos; Lef1; Thbs1; Tnf
MicroRNAs in Cardiomyocyte Hypertrophy	2,86E-02	3,26E-01	5	Cish; Pik3r1; Tnf; Wnt3a; Fzd2
Delta-Notch Signaling Pathway	3,13E-02	3,34E-01	5	Cntfr; Fhl1; Lef1; Pik3r1; Psen2
Endochondral Ossification	4,08E-02	4,11E-01	4	Adamts1; Igf2; Sox6; Thra

SUPRABASAL				
Pathway[2]	**p-value**	**FDR**	**Genes (No.)**	**Genes**
Wnt Signaling in Kidney Disease	7,58E-05	1,30E-02	4	Wnt10b; Wnt3; Wnt4; Wnt7b
Id Signaling Pathway	2,70E-04	2,31E-02	4	Bmp2; Id1; Id3; Smad5
Wnt Signaling Pathway	5,06E-04	2,88E-02	4	Wnt10b; Wnt3; Wnt4; Wnt7b
ESC Pluripotency Pathways	7,74E-04	3,31E-02	5	Smad5; Wnt10b; Wnt3; Wnt4; Wnt7b
Adipogenesis genes	1,38E-03	4,71E-02	5	Bmp2; Socs3; Cntfr; Id3; Wnt10b
Wnt Signaling Pathway and Pluripotency	3,05E-03	8,70E-02	4	Wnt10b; Wnt3; Wnt4; Wnt7b
Hedgehog Signaling Pathway	8,36E-03	2,04E-01	2	Gas1; Igf2
White fat cell differentiation	1,73E-02	3,69E-01	2	Klf2; Wnt10b
Hfe effect on hepcidin production	4,38E-02	8,31E-01	1	Id1

[1]DEG selection criterion: FDR < 0.1
[2]Inclusion criteria: p-value < 0.05
Total number of basal genes: 308
Total number of suprabasal genes:82

ACCEPTED MANUSCRIPT

Table S5. HH, Notch and Wnt signaling pathways gene expression in keratinocytes

ACCEPTED MANUSCRIPT

		BASAL					
		RNA sequencing			Array		
Signaling pathway	**Gene**	**log_2(FC)***	**p-value**	**FDR**	**log_2(FC)***	**p-value**	**FDR**
HH	Bcl2	-0,7403	3,50E-02	3,06E-01	-1,1088	1,28E-01	3,99E-01
	Cdon	-1,6332	1,21E-02	1,29E-01	-1,9858	1,46E-01	4,08E-01
	Gas1	-1,7253	5,00E-05	8,58E-03	-1,2659	2,97E-03	3,56E-01
	Ptch1	-0,6184	2,98E-02	2,71E-01	-1,3423	1,11E-01	3,95E-01
	Ptch2	-1,2418	2,05E-02	2,03E-01	-1,1489	1,88E-01	4,27E-01
Notch	Dvl2	-1,3606	3,13E-02	2,81E-01	-1,1702	1,22E-01	3,98E-01
	Jag2	-0,6350	1,94E-02	1,94E-01	-1,1590	3,49E-02	3,71E-01
	Kat2b	-1,3692	2,32E-02	2,25E-01	-1,0958	4,32E-01	5,26E-01
	Psen2	-4,1669	8,30E-03	9,48E-02	1,0629	2,90E-01	4,69E-01
Wnt	Chd8	-0,8920	1,13E-02	1,22E-01	-1,1466	7,51E-02	3,79E-01
	Csnk1e	-0,9633	2,53E-02	2,41E-01	1,0609	3,40E-01	4,90E-01
	Fzd2	-1,1796	4,30E-03	5,80E-02	1,0383	7,23E-01	6,18E-01
	Fzd5	-1,0225	5,50E-03	7,23E-02	-1,1046	2,95E-01	4,71E-01
	Fzd7	-0,8184	1,08E-02	1,17E-01	1,0441	5,31E-01	5,61E-01
	Fzd8	-2,1543	1,45E-02	1,50E-01	-1,4332	1,05E-02	3,59E-01
	Lef1	-2,0656	5,00E-05	8,58E-03	-1,9617	1,87E-01	4,26E-01
	Myc	-0,5619	5,04E-02	3,95E-01	-1,3342	2,31E-02	3,71E-01
	Nfatc1	-0,5861	3,92E-02	3,31E-01	-1,0229	8,62E-01	6,54E-01
	Prkacb	-1,1216	9,15E-03	1,01E-01	-1,1015	2,43E-01	4,48E-01
	Wnt10b	-1,0441	1,51E-02	1,55E-01	-1,1212	6,02E-01	5,84E-01
	Wnt16	-2,4294	5,00E-05	8,58E-03	-2,3361	1,61E-01	4,14E-01
	Wnt3	-0,6346	2,01E-02	2,00E-01	-1,5306	1,25E-01	3,98E-01
	Wnt3a	-1,7523	1,00E-04	1,35E-02	-1,0501	3,06E-01	4,76E-01
	Wnt4	-0,8524	4,15E-03	5,63E-02	-1,4911	7,38E-02	3,79E-01
	Wnt6	-1,4232	6,50E-04	3,71E-02	-1,1377	4,29E-01	5,25E-01
	Wnt7b	-0,7942	6,55E-03	8,49E-02	-1,1416	3,52E-01	4,95E-01

		SUPRABASAL					
		RNA sequencing			**Array**		
Signaling pathway	**Gene**	**log_2(FC)***	**p-value**	**FDR**	**log_2(FC)***	**p-value**	**FDR**
HH	Arrb1	-1,8913	2,33E-02	3,37E-01	-1,0498	7,14E-01	8,10E-01
	Cdon	-1,8857	4,70E-03	1,41E-01	-1,7778	2,30E-01	7,01E-01
	Gas1	-1,3122	5,00E-04	6,31E-02	-1,0822	1,57E-01	6,80E-01
Notch	Dtx2	-0,7487	3,18E-02	4,06E-01	-1,2931	6,97E-02	6,54E-01
	Hes1	-0,7231	3,56E-02	4,30E-01	-1,4745	1,66E-01	6,81E-01
	Notch3	-1,1697	1,10E-03	1,10E-01	-1,3689	2,08E-01	6,93E-01
Wnt	Fosl1	-1,2175	2,35E-03	1,41E-01	-1,4263	2,73E-01	7,12E-01
	Frat1	-2,6110	3,53E-02	4,28E-01	-1,0571	1,21E-02	5,99E-01
	Frat2	-1,2847	1,68E-02	2,65E-01	-1,3123	7,47E-02	6,57E-01
	Jun	-1,4860	3,75E-03	1,41E-01	-1,4082	2,02E-01	6,92E-01
	Vangl2	-0,8748	2,18E-02	3,23E-01	-1,2436	1,03E-01	6,62E-01
	Wnt10a	-1,4703	6,00E-03	1,41E-01	-1,0847	5,12E-01	7,71E-01
	Wnt10b	-3,2272	7,00E-04	8,24E-02	-1,3330	1,20E-01	6,71E-01
	Wnt16	-2,7418	5,55E-03	1,41E-01	-1,9086	1,55E-01	6,80E-01
	Wnt3	-1,4183	8,50E-04	9,29E-02	-1,4916	3,65E-01	7,36E-01
	Wnt4	-1,6223	5,00E-05	1,61E-02	-1,4310	1,85E-01	6,86E-01
	Wnt6	-1,4761	1,47E-02	2,43E-01	-1,1948	2,72E-01	7,12E-01
	Wnt7b	-1,8351	5,00E-05	1,61E-02	-1,2702	2,65E-02	6,10E-01

Figure S1. Progerin expression leads to downregulation of stem cell markers.
(a) FACS plot showing the gating used to sort basal ($CD45^{neg}/CD49f^{high}$) and suprabasal ($CD45^{neg}/CD45^{low}$) keratinocytes. **(b)** Plot of top 20 GO terms showing biological processes with a threshold of p-value < 0.05 and FDR < 0.1. Processes related to skin development and differentiation are shown in blue. Other non-related processes are shown in pink. **(c-d)** Volcano plot showing the changes in gene expression in HGPS relative to wild-type mice in the different types of basal (c) and suprabasal (d) keratinocytes. **(e-f)** Heatmap comparison of RNA sequencing data with expression array data in hair follicles (e) and IFE (f) keratinocytes. Genes analyzed for the different cell populations are represented as log2(fold change) and were selected based on a threshold of p-value < 0.05. **(g)** K15 *in situ* hybridization on PD4 HGPS and wild-type skin. **(h)** K15 dots per cell quantification in HGPS and wild-type skin at E18.5 and PD4 (n = 3/group). Data are represented as mean ± SEM. Scale bars: (g) = 100μm.

Figure S2. Unaltered epigenetic regulators of keratinocytes differentiation in HGPS mice skin.
(a) Volcano plot representing epigenetic regulators involved in keratinocytes proliferation and differentiation analyzed for changes in gene expression between wild-type and HGPS mice. **(b)** Differentially expressed epigenetic regulators in basal and suprabasal keratinocytes. $Log_2(FC)$ = log2(fold change).

Figure S3. Wnt signaling is downregulated in HGPS suprabasal keratinocytes
(a-b) Volcano plot showing Notch, Wnt and HH signaling pathways in basal (a) and suprabasal (b) keratinocytes analyzed for changes in gene expression between wild-type and HGPS mice. **(c-d)** Genes analyzed for the different basal (c) and suprabasal (d) cell populations are represented as log2(fold change) and were selected based on a threshold of p-value < 0.05.

Figure S4. HGPS patient fibroblasts show reduced β-catenin levels. Patient and control fibroblasts were supplemented with 150ng/ml Wnt3a over a 24-hour time course. **(a)** Nuclear β-catenin protein levels were measured at 0, 8, 16 and 24-hours after stimulation by western blot. β-actin was used as loading control. **(b)** Graph showing the normalized protein levels at the different time points. **(c)** Immunofluorescent staining of active β-catenin (red) after 8 hours of Wnt3a stimulation of fibroblasts. **(d)** Graph representing the fluorescence intensity of active β-catenin in cell nuclei before and after 8 hours of stimulation. **(e)** Axin2 mRNA expression was evaluated before and after 8 hours of stimulation in control and HGPS cells. Data are represented as mean ± SEM. Scale bar: (c) = 10μm.

ACCEPTED MANUSCRIPT

ACCEPTED MANUSCRIPT

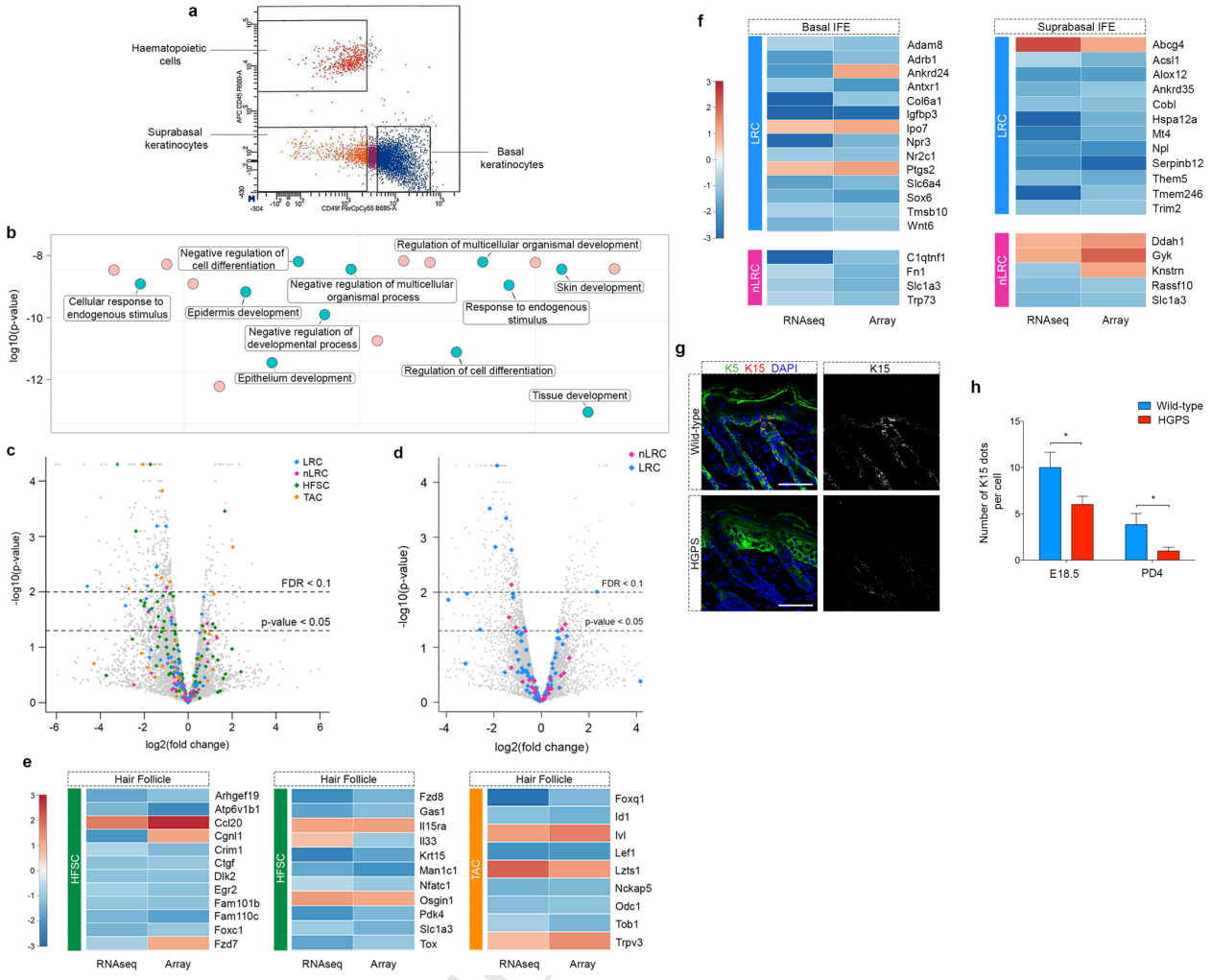

a

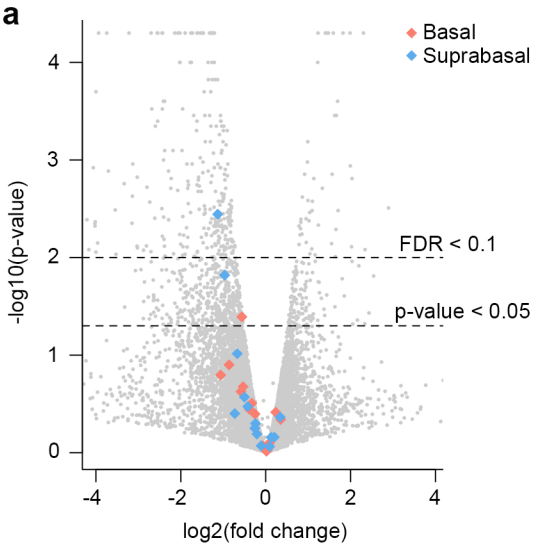

b

BASAL

Epigenetic regulator genes	log_2(FC)	p-value
Actl6a	0,0376	0,9359
Bmi1	-0,8636	0,1258
Cbx2	-0,5331	0,2106
Eed	0,0183	0,9653
Ezh1	-0,5823	0,2364
Ezh2	-0,3850	0,3582
Gadd45a	0,0866	0,7966
Gadd45b	-0,2517	0,4010
Hdac1	-1,0609	0,1600
Hdac2	0,2354	0,3845
Pcgf2	-0,3273	0,3111
Satb1	-0,5618	0,0406
Setd8	-0,0728	0,8544
Uhrf1	0,3531	0,4565

SUPRABASAL

Epigenetic regulator genes	log_2(FC)	p-value
Actl6a	-0,1076	0,8498
Bmi1	-0,2060	0,6439
Cbx2	-0,2556	0,5620
Eed	0,0939	0,8659
Ezh1	0,2026	0,6927
Ezh2	-0,4209	0,3367
Gadd45a	-0,5008	0,2693
Gadd45b	-1,1301	0,0036
Hdac1	-0,7286	0,3972
Hdac2	-0,2401	0,5027
Pcgf2	-0,6703	0,0966
Satb1	-0,9662	0,0152
Setd8	0,1298	0,6957
Uhrf1	0,3412	0,4317

ACCEP

ACCEPTED MANUSCRIPT

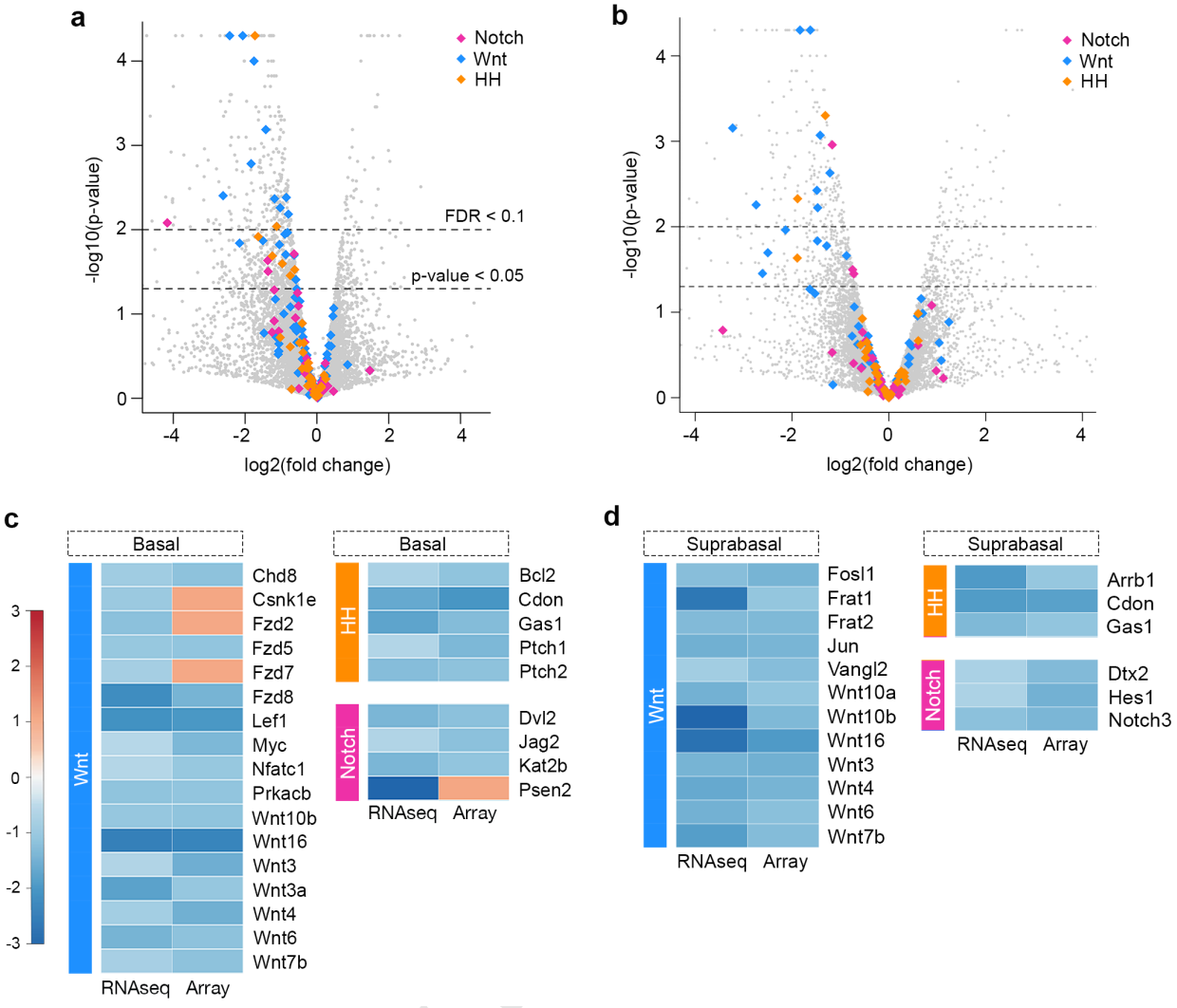

ACCEPTED

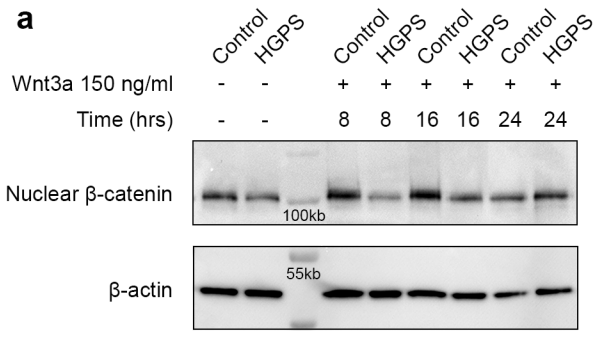
a
Control
HGPS
Control
HGPS
Control
HGPS
Control
HGPS
Wnt3a 150 ng/ml
- - + + + + + +
Time (hrs)
- - 8 8 16 16 24 24
Nuclear β-catenin
100kb
β-actin
55kb

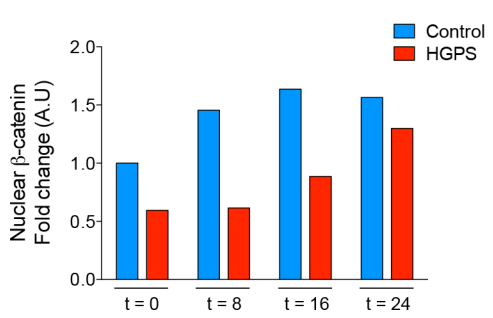
b
Control
HGPS
Nuclear β-catenin
Fold change (A.U)
2.0
1.5
1.0
0.5
0.0
t = 0
t = 8
t = 16
t = 24

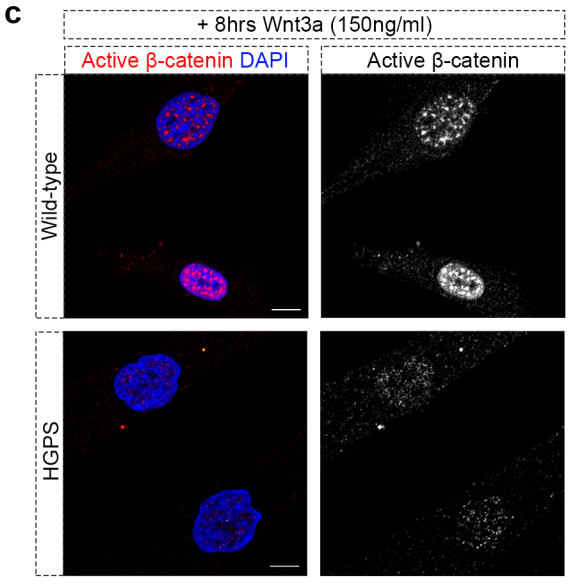
c
+ 8hrs Wnt3a (150ng/ml)
Active β-catenin DAPI
Active β-catenin
Wild-type
HGPS

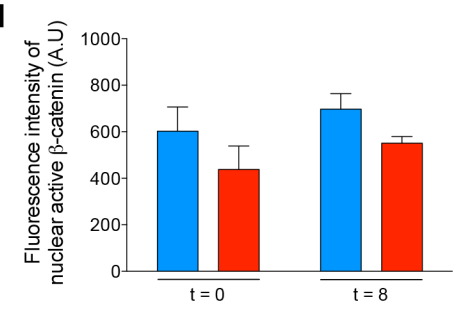
d
Fluorescence intensity of
nuclear active β-catenin (A.U)
1000
800
600
400
200
0
t = 0
t = 8

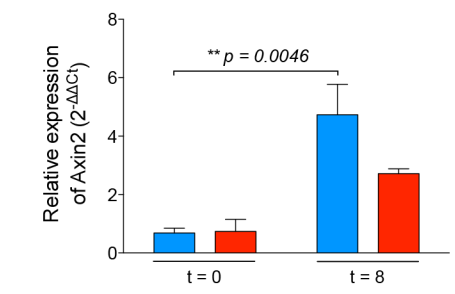
e
Relative expression
of Axin2 (2-ΔΔCt)
** p = 0.0046
8
6
4
2
0
t = 0
t = 8

ACCEPTED